Mapping amoeboid cell migration

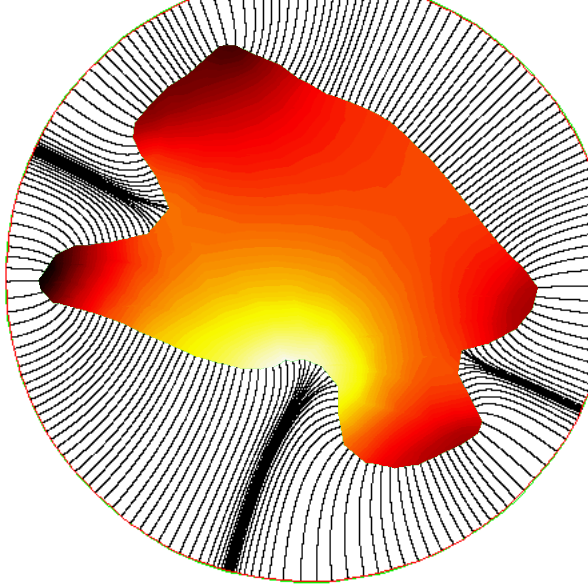

Till Bretschneider
Warwick Systems Biology Centre

InnoMol BioImaging workshop 22nd October 2014, Ruđer Bošković Institute, Zagreb

THE UNIVERSITY OF WARWICK

Outline

Part I: Methods (LineageTracker, CellTracker, QuimP)

- Introduction to graph based approaches for multi cell (point) tracking and image segmentation
- Surface matching: Tackling biological shape variability (active contour based methods)
- Utilising inexpensive GPU computing for fast 3D real time imaging of Light Sheet Microscopy Data

Part II: Applications: Tracking spatio-temporal fluorescence distributions in migrating cells

- Biochemistry: Fitting mathematical models for cell reorientation to time series image data
- Cellular Mechanics: Blebbing

- Zatulovskiy E, Tyson R, Bretschneider T, Kay RR. Bleb-driven chemotaxis of Dictyostelium cells. J Cell Biol. 2014 Mar 17;204(6):1027-44.
- Tyson RA, Zatulovskiy E, Kay RR, Bretschneider T. How blebs and pseudopods cooperate during chemotaxis. Proc Natl Acad Sci U S A. 2014 Aug 12;111(32):11703-

WARWICK

Cell tracking using multi feature global optimisation

- LineageTracker: ERASysBio project to investigate the connection between the cell cycle and the clock using FUCCI markers (tracking cell nuclei)

  Feillet C, Krusche P, Tamanini F, Janssens RC, Downey MJ, Martin P, Teboul M, Saito S, Lévi FA, Bretschneider T, van der Horst GT, Delaunay F, Rand DA. Phase locking and multiple oscillating attractors for the coupled mammalian clock and cell cycle. Proc Natl Acad Sci U S A. 2014 Jul 8;111(27):9828-33.

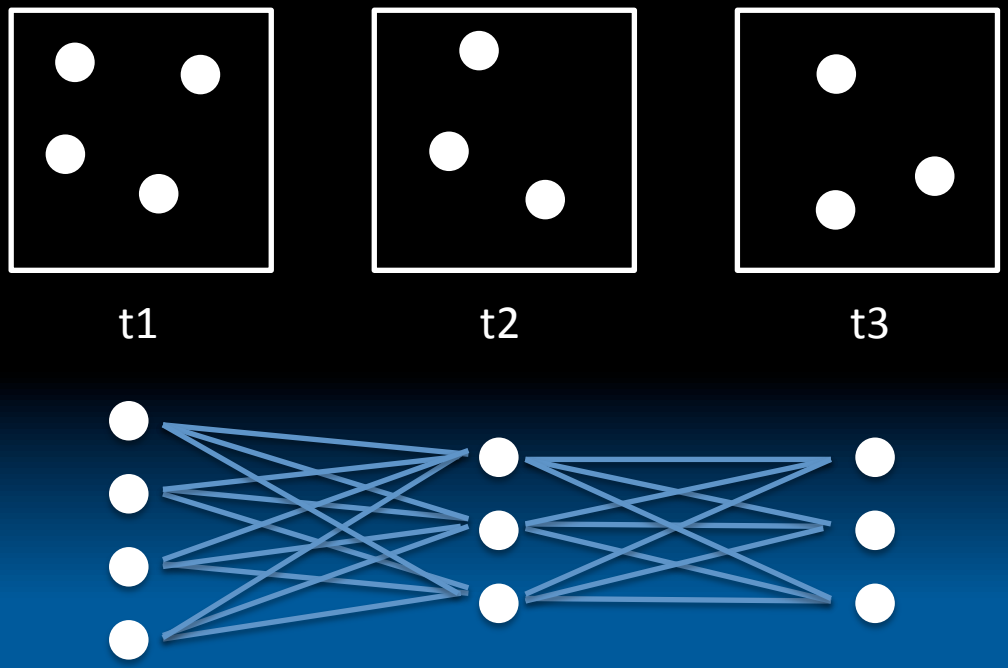

Graph: consists of nodes (vertices) and edges

Weight matrix W: edges weighted according to similarity of nodes

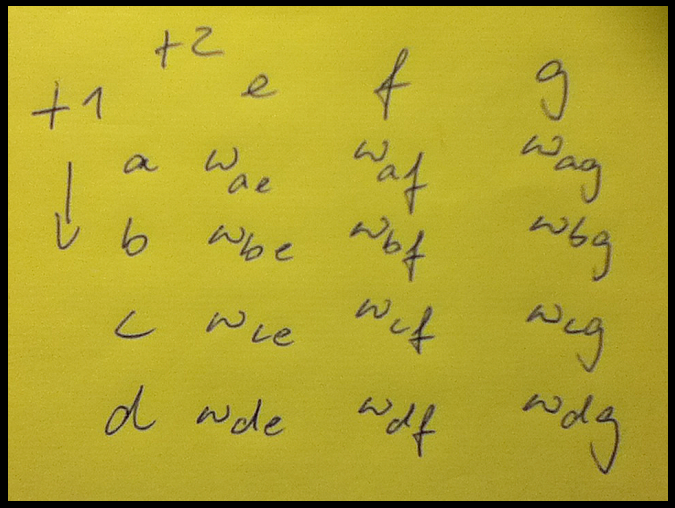

Similarity (weight) matrix can account for multiple features:

- distance of cells
- differences in brightness, area, shape
- cell state (dividing, post division)
- multiple channel information …

Weights describe the probability P that two cells at subsequent time points are identical.

P can be converted into a cost (1-P). Standard methods from linear algebra for minimising the total cost exist (Hungarian algorithm and derivates)

Adjacency matrix A captures the structure of the graph

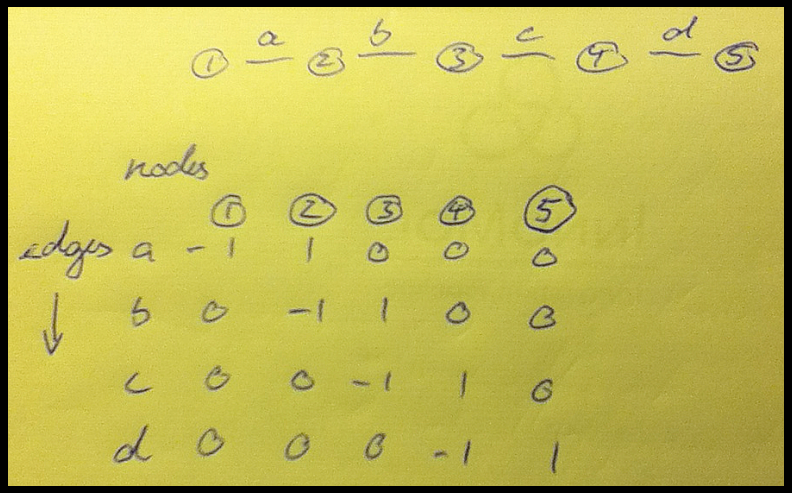

Constitutive matrix C containing weights for each edge

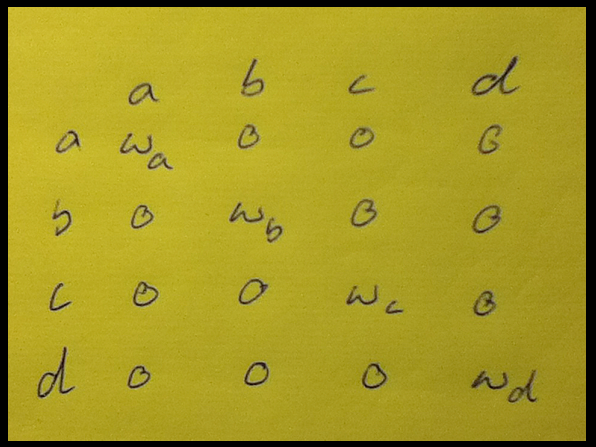

The graph Laplacian matrix $L=A^TCA$ incorporates both, the structure and weights

L is the discrete version of the continuous Laplace operator

$$L = \text{div grad} = \delta^2/\delta x^2$$

Random walks for image segmentation

Graph Laplacian L = div grad = $\delta^2/\delta x^2$

L is associated with diffusion problems or random walks.

Fick's 2nd law of diffusion: $\delta u/\delta t = D\ \delta u^2/\delta x^2$

u: concentration, electric potential, temperature, image brightness

Laplace's equation: $\delta u^2/\delta x^2 = 0$ (stationary)

Laplace's equation can be solved by minimizing the Dirichlet integral (potential energy). In effect, diffusion smoothens out all gradients.

Dirichlet integral $$D[u] = \frac{1}{2}\int_\Omega |\nabla u|^2 d\Omega$$ where ∇ = grad

The corresponding problem on a graph is solved by finding:

$$\min \tfrac{1}{2}\, u^T L u = \tfrac{1}{2} \Sigma\, |u_i - u_j|^2$$

with suitable boundary conditions

Supervised segmentation: user provide boundary conditions (partitioning of a graph)

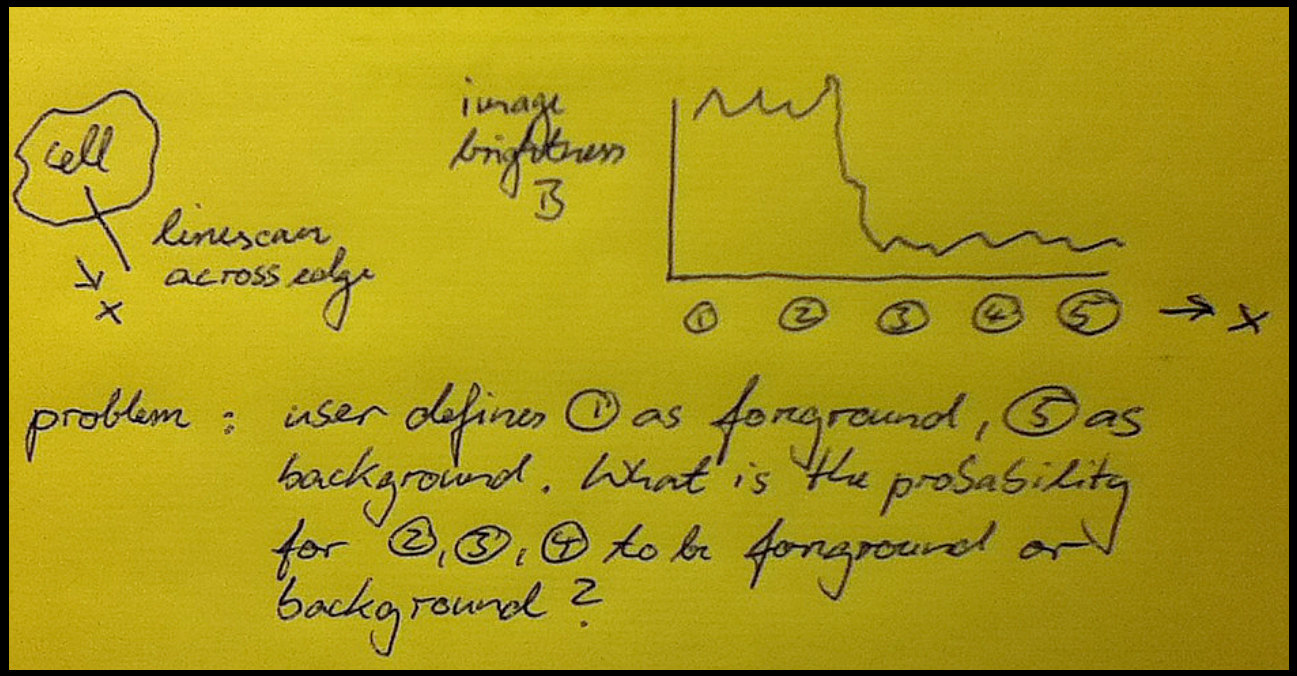

Consider diffusion on the graph with node 1 as source and node 5 as sink. Diffusion is limited across edges with low similarity, ie where we have steps in the image. Anisotropic diffusion preserves edges.

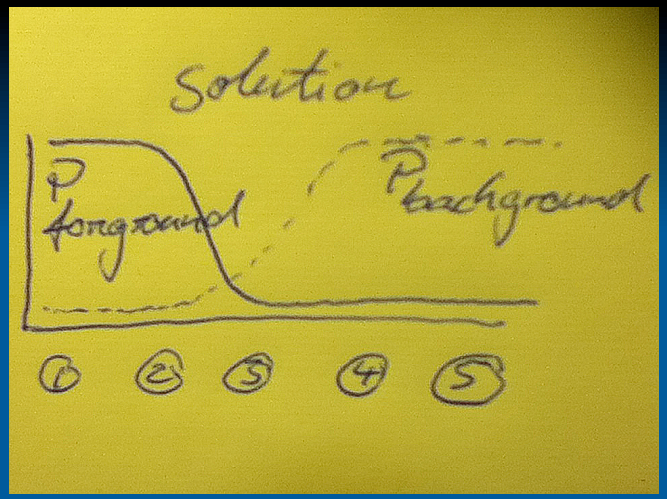

$P_{fg} > P_{bg}$: assign pixel to foreground
$P_{bg} > P_{fg}$: assign pixel to background

Probabilistic framework allows to put confidence limits on segmentation, for example to restrict processing to regions of high confidence

Advantages of the random walk segmentation (and its many variants)

- Multi object segmentation possible (cell cluster)
- Enables neutral segmentation (separating cells with identical intensities)
- Works in 3D
- Multiple features can be integrated (intensity, texture, multiple colour channels, …)
- Computationally very efficient
- Sound theoretical basis

CellTracker software: Measuring nucleus-cytoplasmic translocations of transcription factors

Xue M, Momiji H, Rabbani N, Barker G, Bretschneider T, Shmygol A, Rand D, Thornalley PJ. Frequency modulated translocational oscillations of Nrf2 mediate the ARE cytoprotective transcriptional response. Antioxid Redox Signal. 2014 Sep 2. [Epub ahead of print]

3D analysis of neutrophil motility using Laplacian approaches

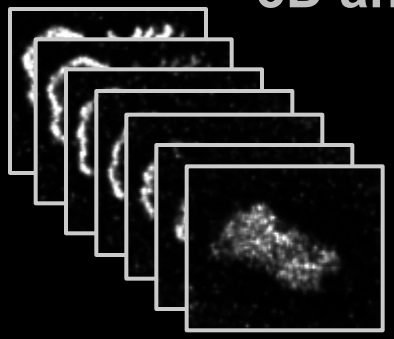

Segmentation

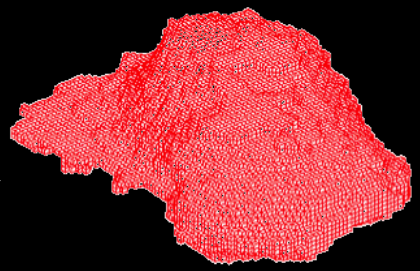

Pre-processing

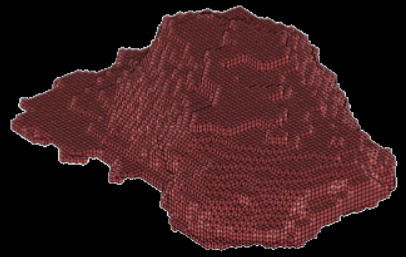

with Len Stephens & Phil Hawkins, Babraham

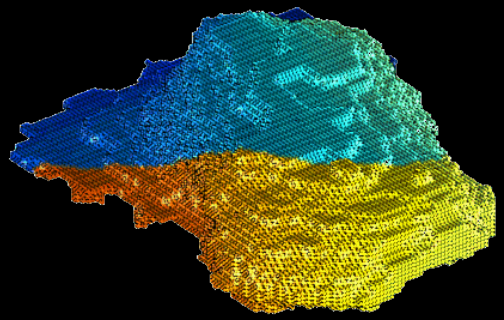

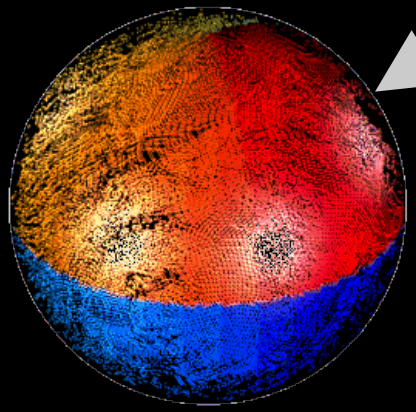

Spherical parameterization

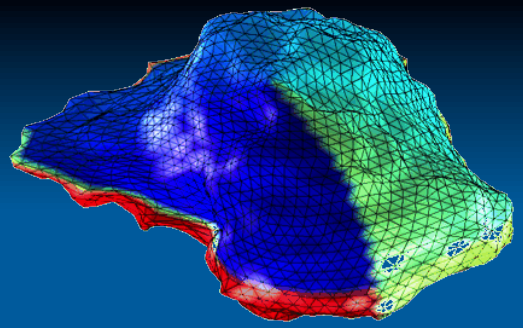

Surface expansion

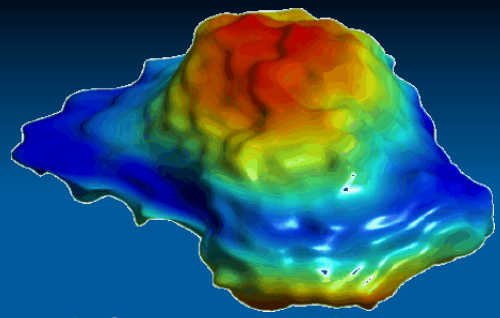

Shape analysis

Du et al., Cytometry A, 2010
Du et al., ISBI 2011
Du et al., ISBI 2012
Du et al., BMVC 2012
Du et al., BMC Bioinformatics, 2013

Quantifying shape deformations

Problem: find corresponding nodes on two surface meshes

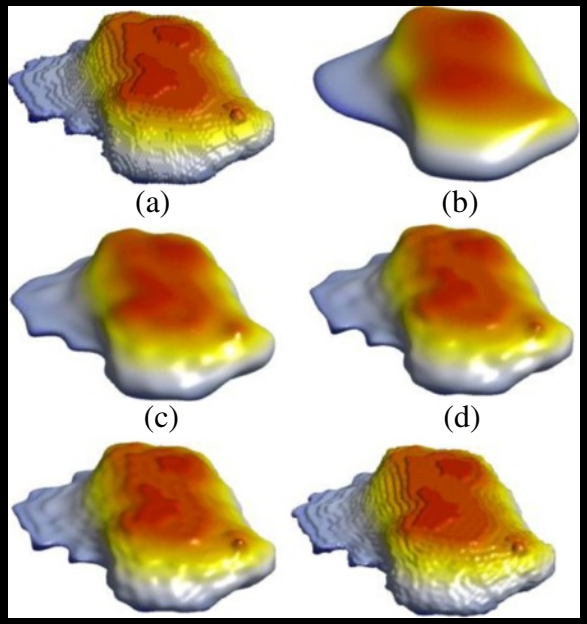

- Rigid transformations
- Using fiducial markers
- 3D shape matching using spherical parameterisation
- Direct feature matching (curvature/intensity, …) using spectral coordinates (modes/eigenvectors of the graph Laplacian) to constrain the problem (regularisation)
- Deformable contours/surfaces (QuimP)

Spectral alignment methods

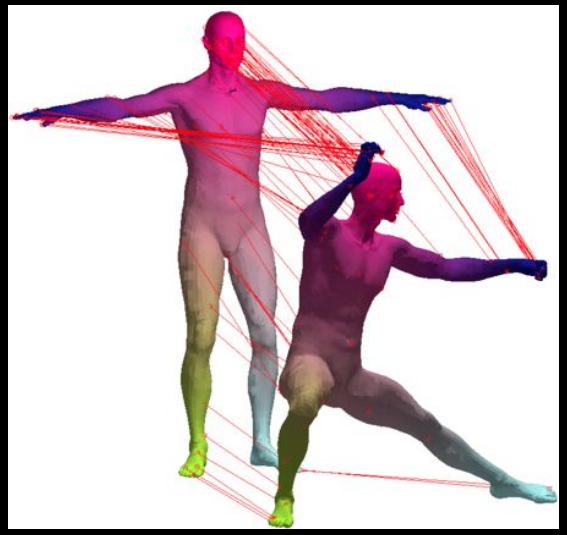

FOCUSR: Feature Oriented Correspondence Using Spectral Regularization--A Method for Precise Surface Matching

Herve Lombaert, Leo Grady, Jonathan R. Polimeni, Farida Cheriet
Pattern Analysis and Machine Intelligence, IEEE Transactions on , vol.35, no.9, pp. 2143,2160, Sept. 2013

Eigendecomposition of the graph Laplacian matrix it its eigenmodes (eigenvectors) reveals strong correspondences between shapes

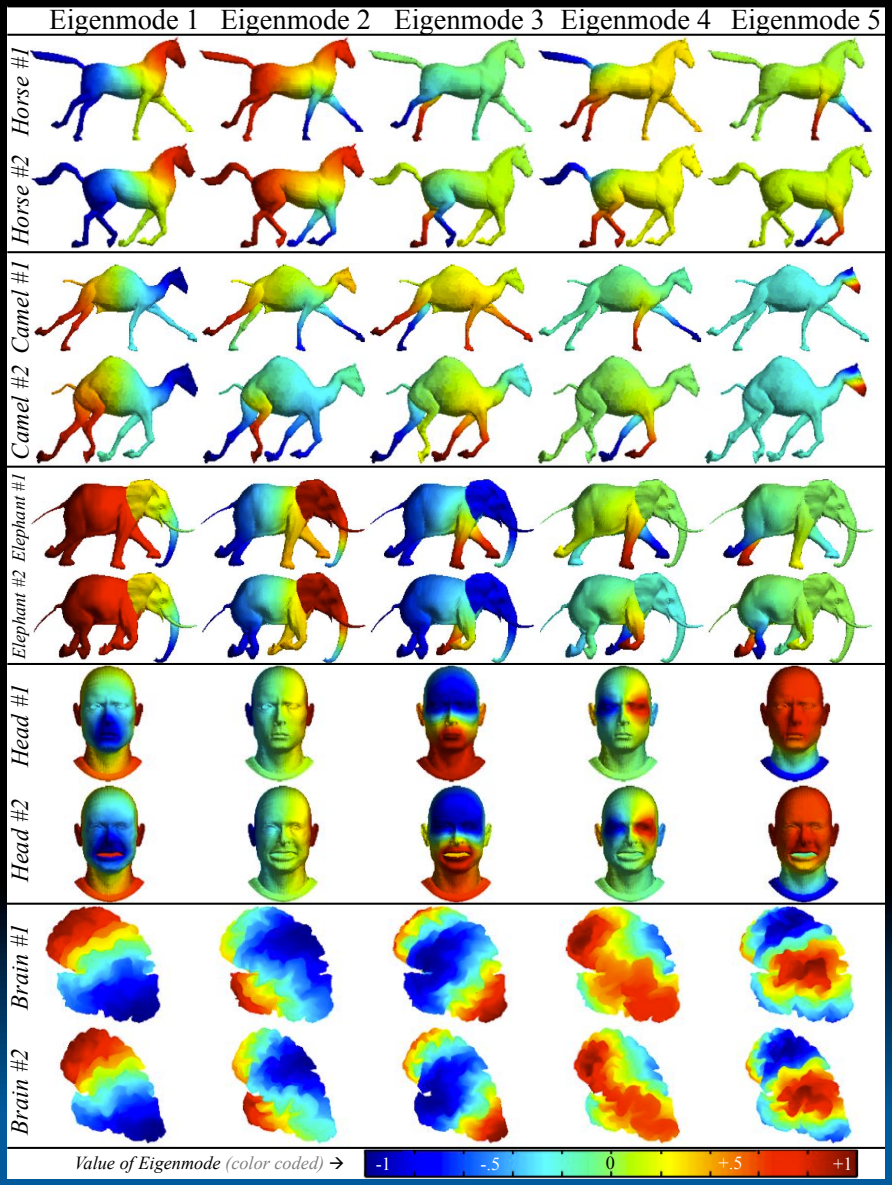

Fig. 1. Example of eigenmodes for pairs of animals and human brain surfaces. Each row shows the first five spec- tral components of a model (eigenmodes of the associated graph Laplacian, reordered and sign adjusted, so paired sets match). The color scale indicates the value of the spectral coordinate over the surface.

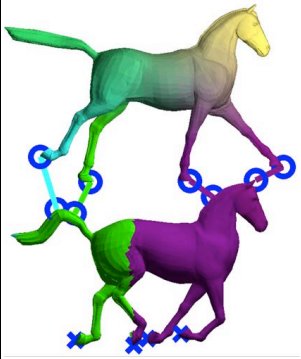

For all points v_i:
$\mathbf{X}_i = (x,y,z)_i$
↓
Closest points
in space:
$\min_\phi \| \mathbf{X}_i - \mathbf{Y}_{\phi(i)} \|$
↓
Corresponding points:
$\mathbf{X}_{\phi(i)} = (x,y,z)_{\phi(i)}$

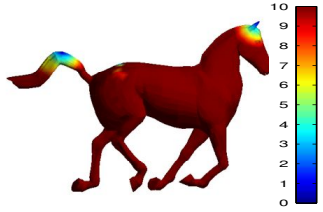

Relative error of the
Correspondence map
(in %, lower the better)

Correspondence using
Closest points in space
(wrong matching)

For all points v_i:
$\mathcal{X}_i = (\mathbf{x}^{(1)}, \mathbf{x}^{(2)}, \mathbf{x}^{(3)})_i$
↓
Closest points
in spectral domain:
$\min_\phi \| \mathcal{X}_i - \mathcal{X}_{\phi(i)} \|$
↓
Corresponding points:
$\mathcal{X}_{\phi(i)} = (\mathbf{x}^{(1)}, \mathbf{x}^{(2)}, \mathbf{x}^{(3)})_{\phi(i)}$

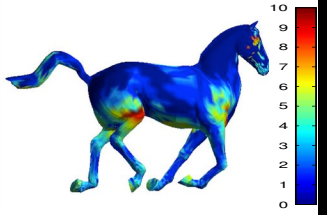

Relative error of the
Correspondence map
(in %, lower the better)
Average error: 2.02%

(a) Finding closest poin

3D

domain (matched legs)

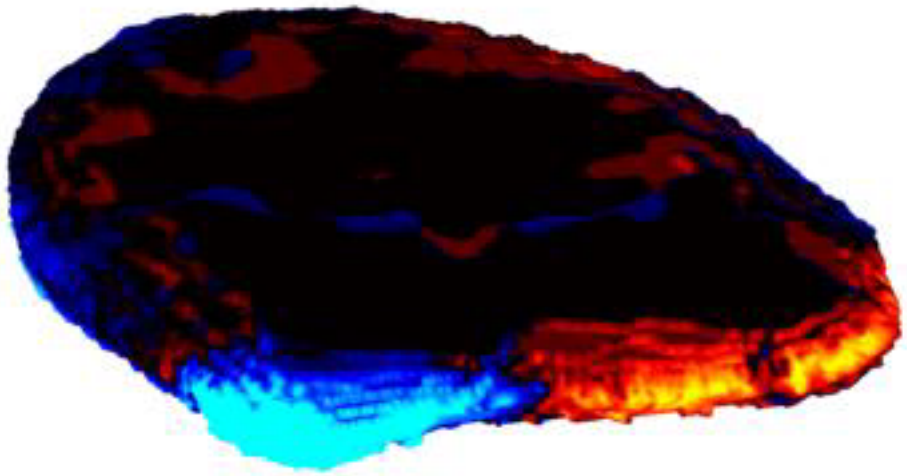

Correspondence using
FOCUSR
(improved matching)

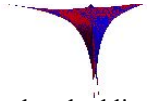

Spectral embeddings in 3D
$\mathcal{X}$ *(red) and* $\mathcal{Y}$ *(blue)*

Correspondence map
(in %, lower the better)
Average error: 1.46%

WARWICK

QuimP: ImageJ plugins for quantifying cellular morphodynamics

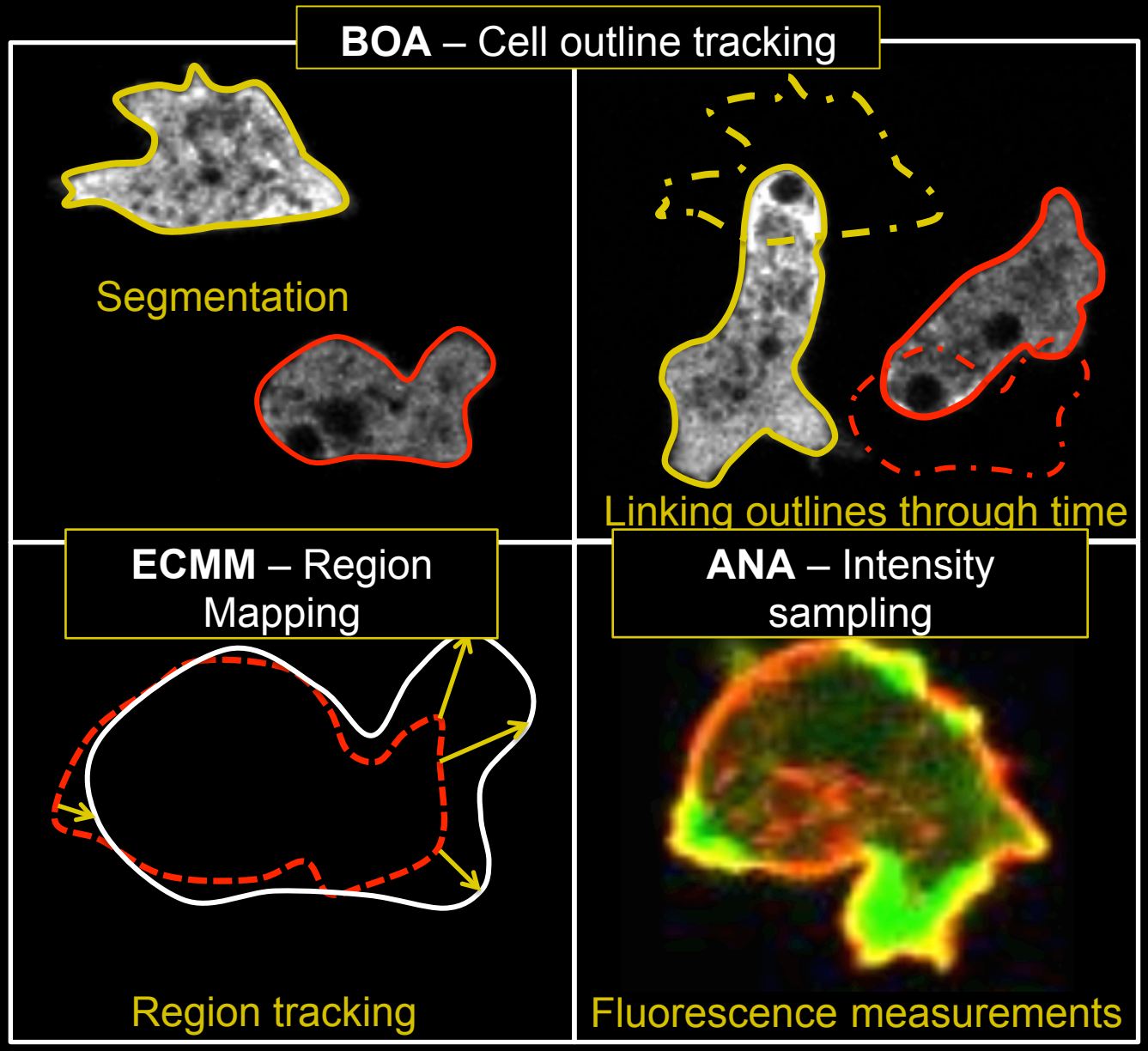

Dormann et al., Cell Motil. Cytoskeleton, 2002; Bosgraaf et al., ibid., 2009

go.warwick.ac.uk/quimp

Active contour based methods for automated cell outline detection

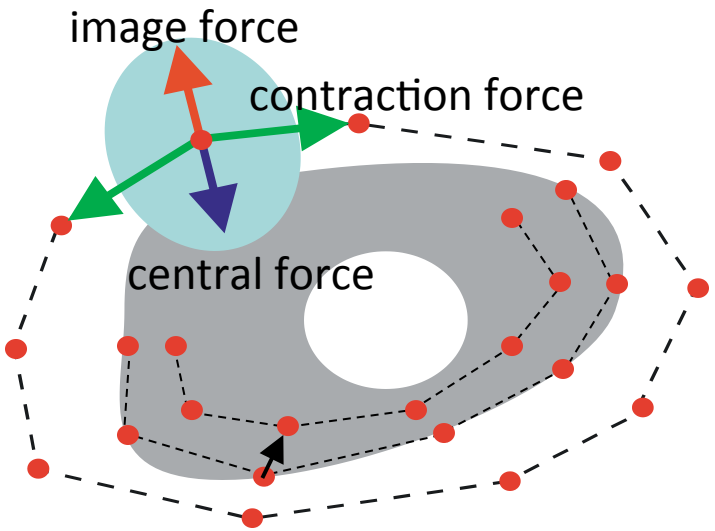

$$\vec{F}_i = Z * \vec{F}_i^{central} \cdot K * \vec{F}_i^{contraction} \cdot B * \triangle h_i \vec{F}_i^{image} \cdot \vec{F}_i^{friction} \quad (1)$$

$$m * \dot{\vec{v}}_i^t = \vec{F}_i^t \quad (2)$$

$$\vec{v}_i^{t \cdot dt} = \vec{v}_i^t \cdot \vec{F}_i^t * dt \quad (3)$$

$$\vec{x}_i^{t \cdot dt} = \vec{x}_i^t \cdot \vec{v}_i^{t \cdot dt} * dt \quad (4)$$

The truncation criterion is fulfilled, when $\vec{v}_i^t < trunc$.

Dormann, Libotte, Weijer & Bretschneider, Cell Mot. Cytoskeleton, 2002

Electrostatic Contour Mapping Method

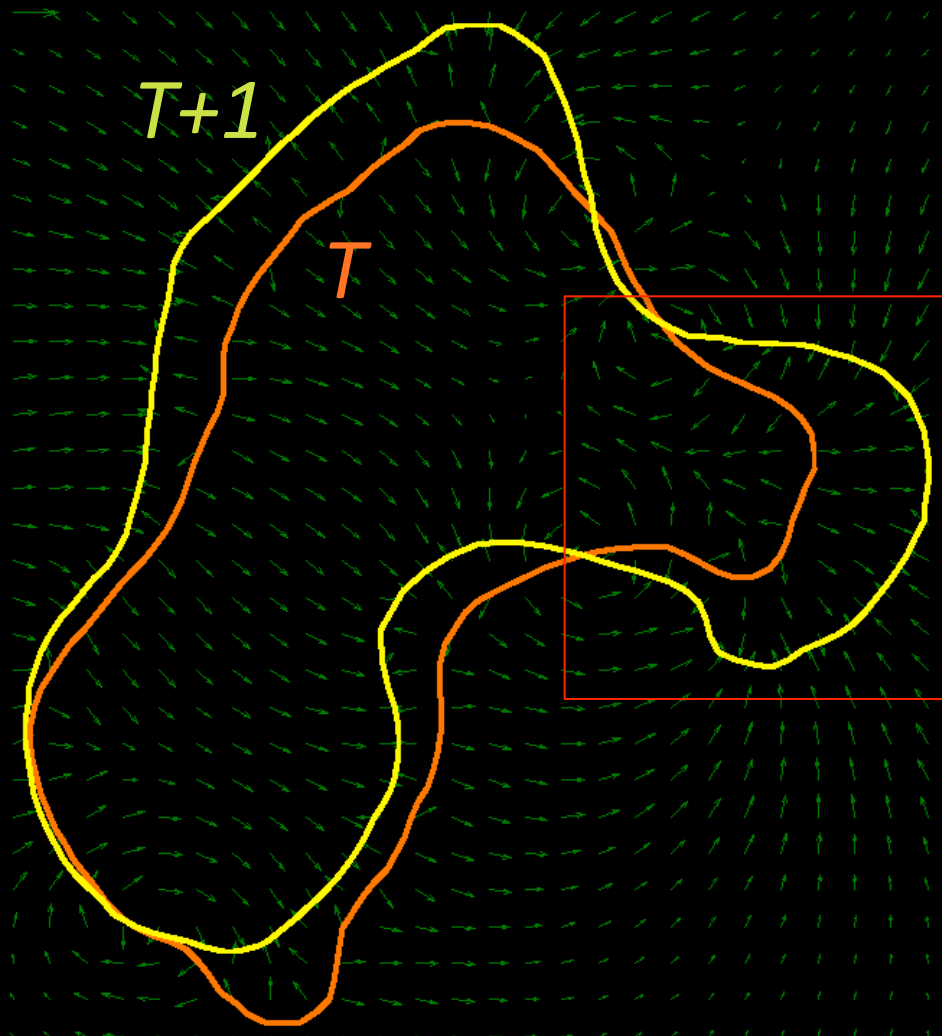

Field lines do not cross

Tyson et al.: High Resolution Tracking of Cell Membrane Dynamics in Moving Cells
Math. Model. Nat. Phenom. Vol. 5, No. 1, **2010**

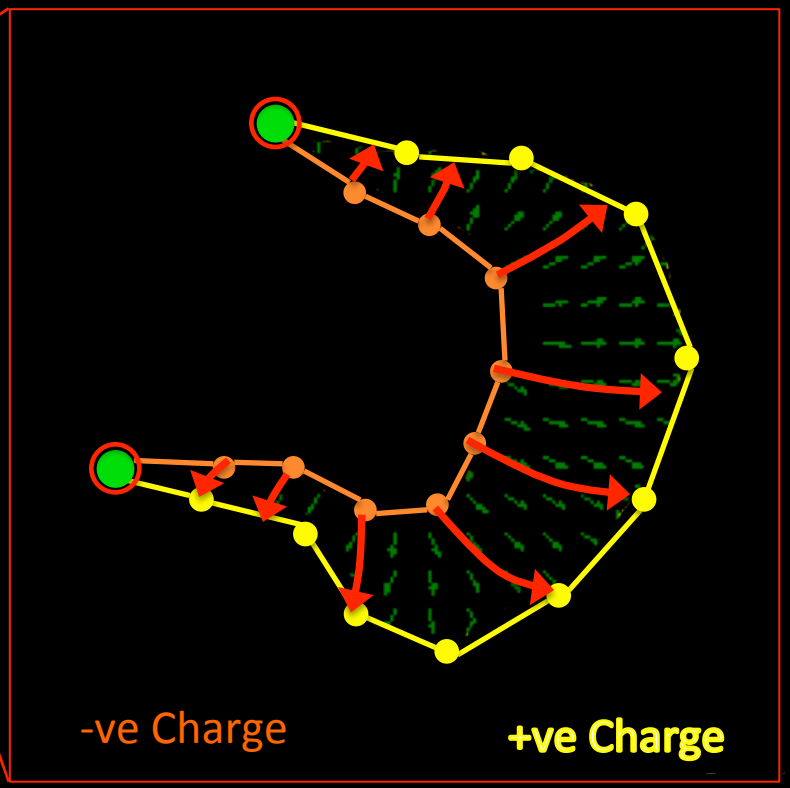

Light Sheet Fluorescence Microscopy

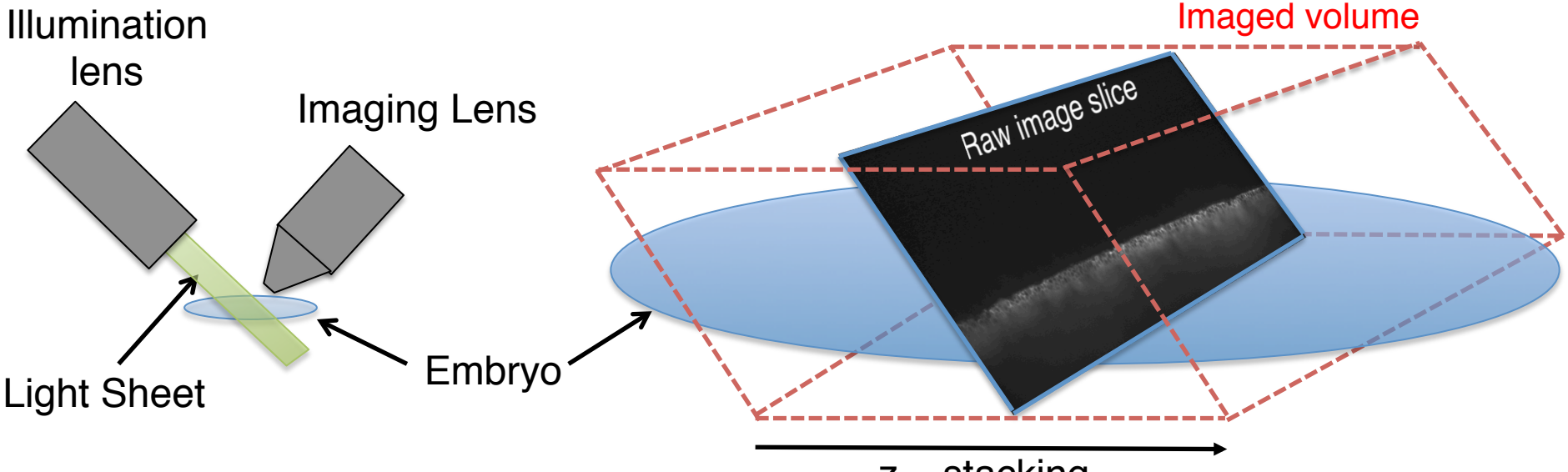

188 sec frame interval
(~12 hour imaging time)

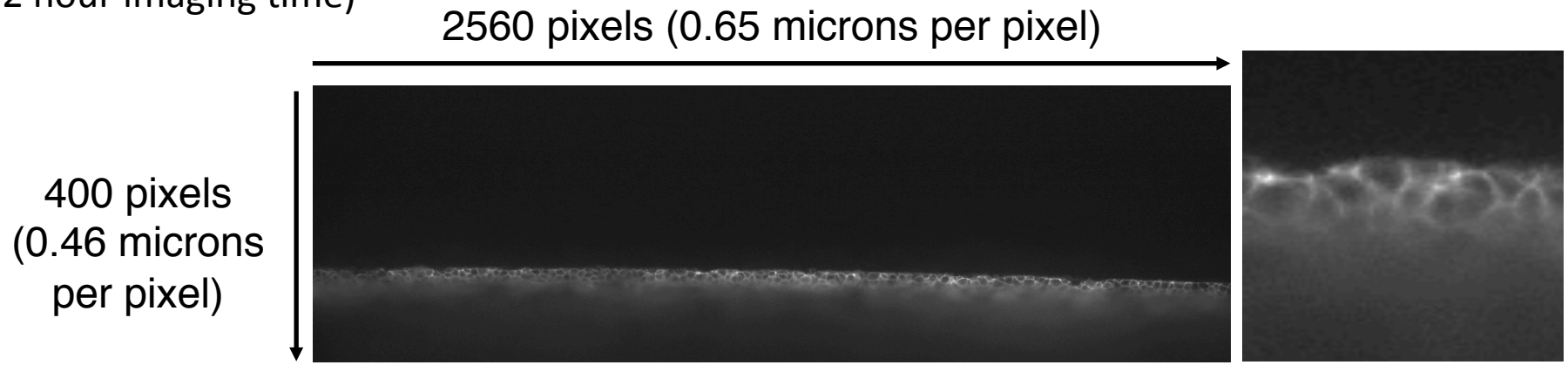

Adding GPU capabilities – Netstore NA255A

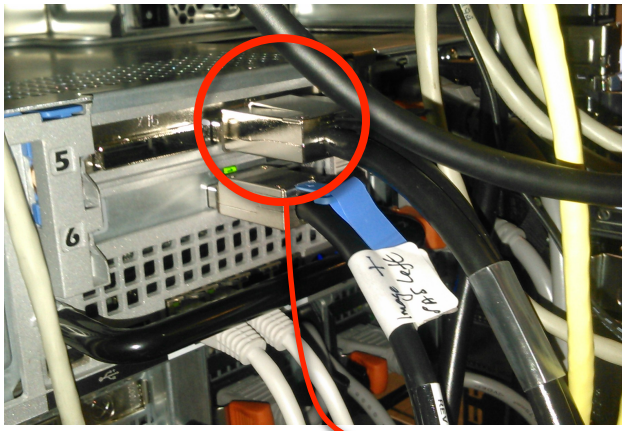

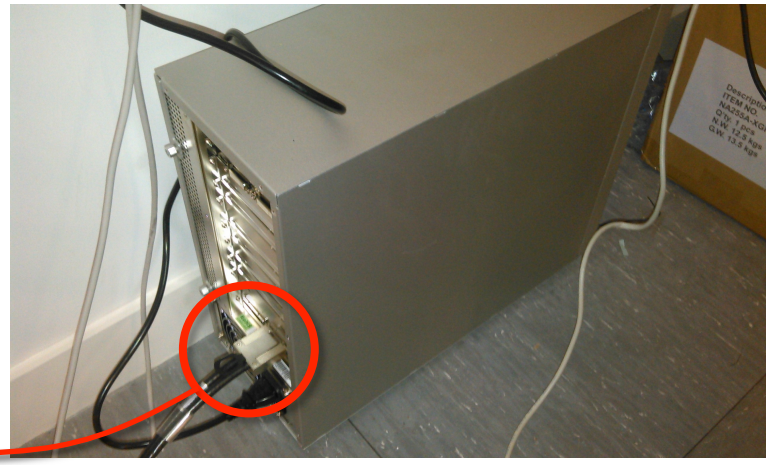

PCI express 3.0

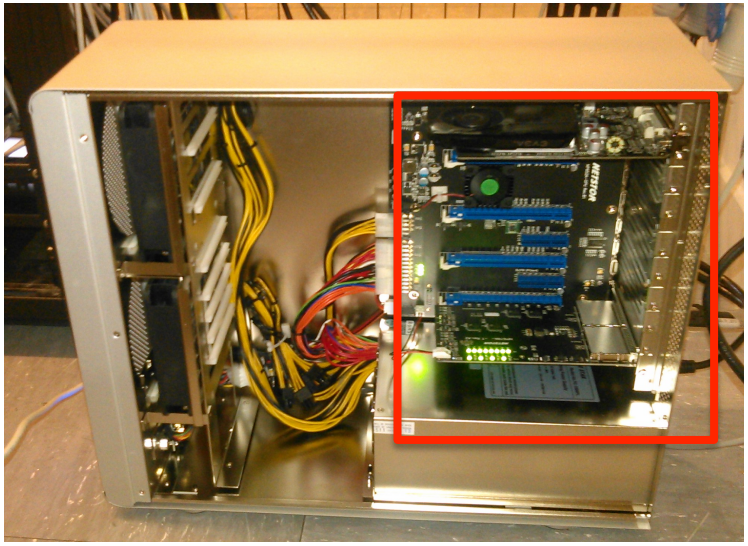

4 GPUs share bandwidth ≈ 16,000 MB/s (16 GB/s)

Available to all remote users

Surface detection

Iteratively warp sampling windows to the surface. Score intensity, variance, and ‘sharpness’ (via FFT transform)

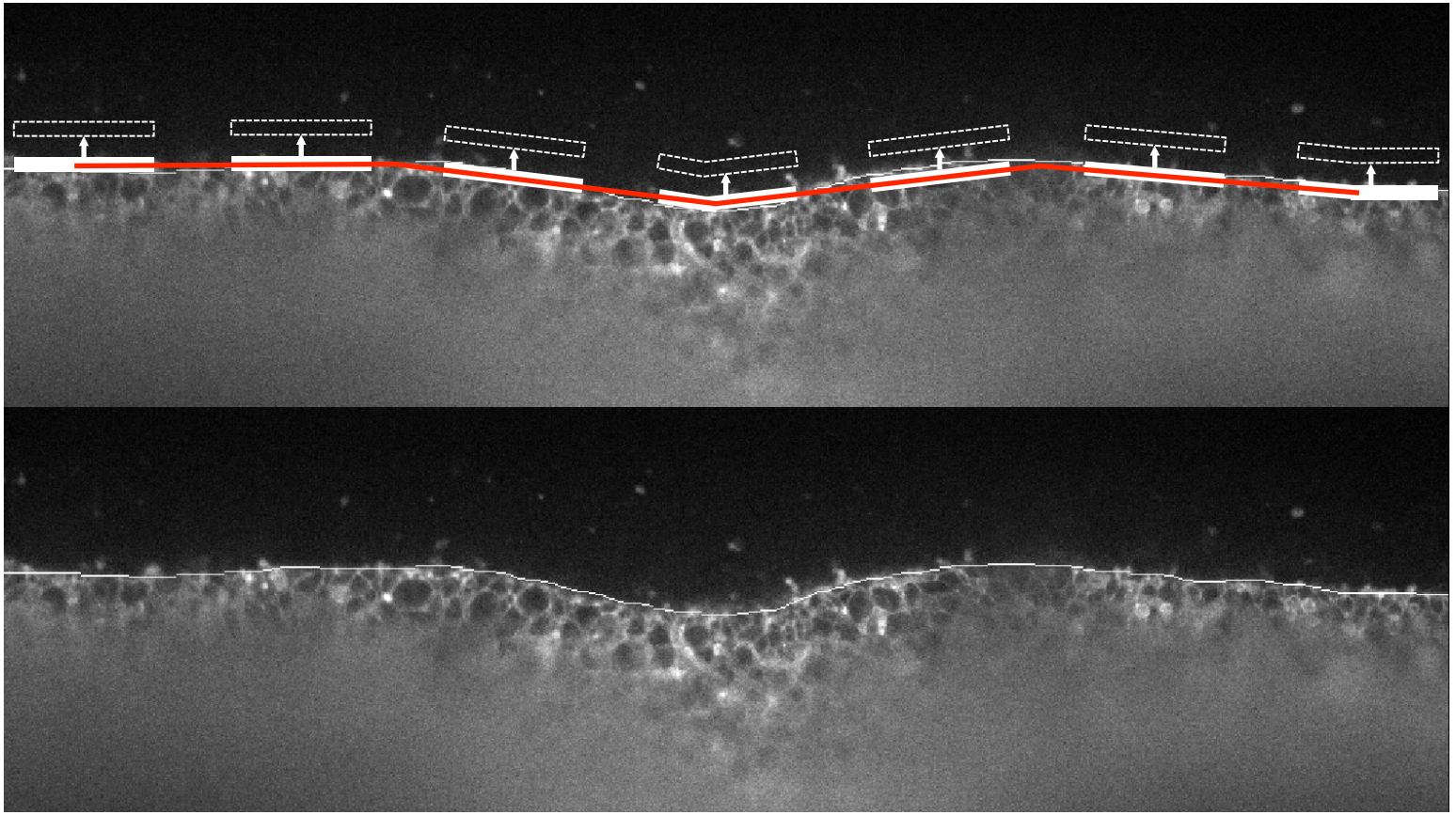

Flow analysis using local registration

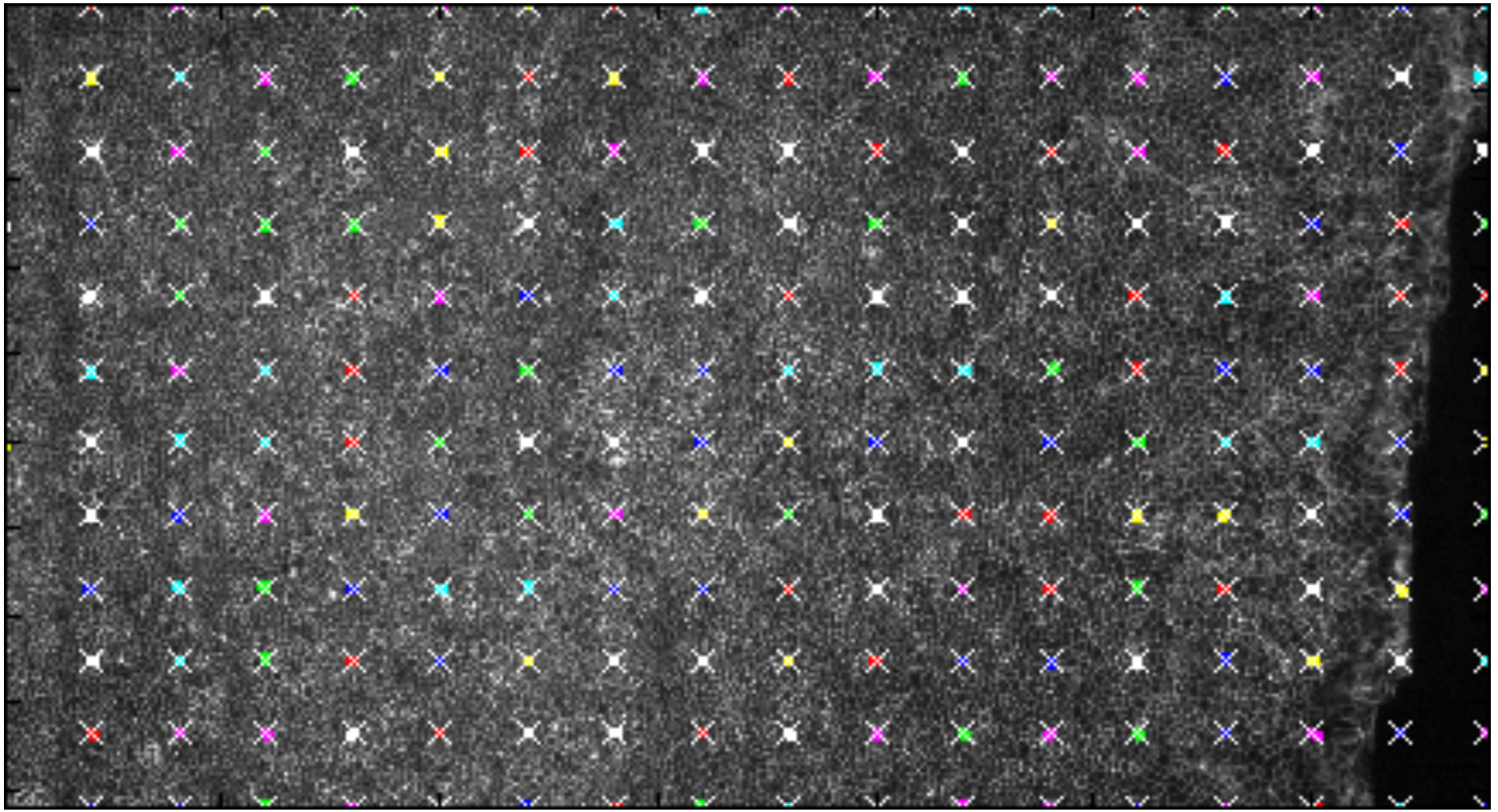

3D visualisation

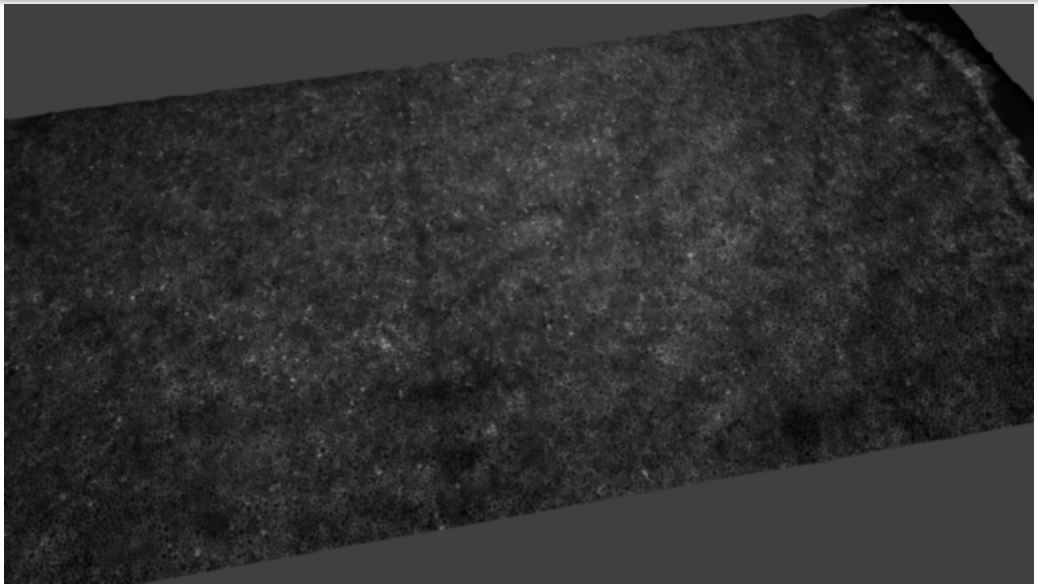

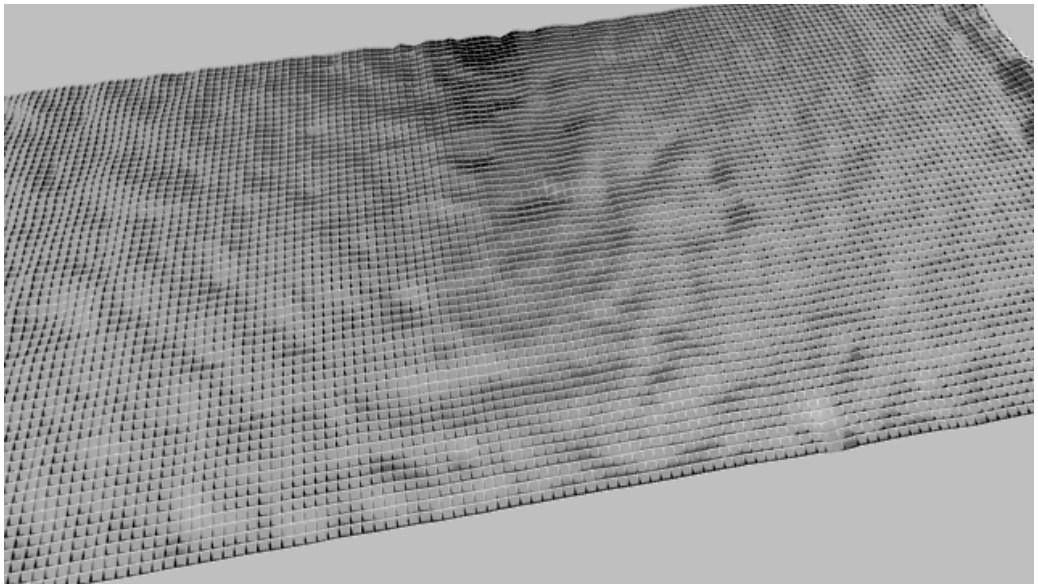

Real Time Tracking

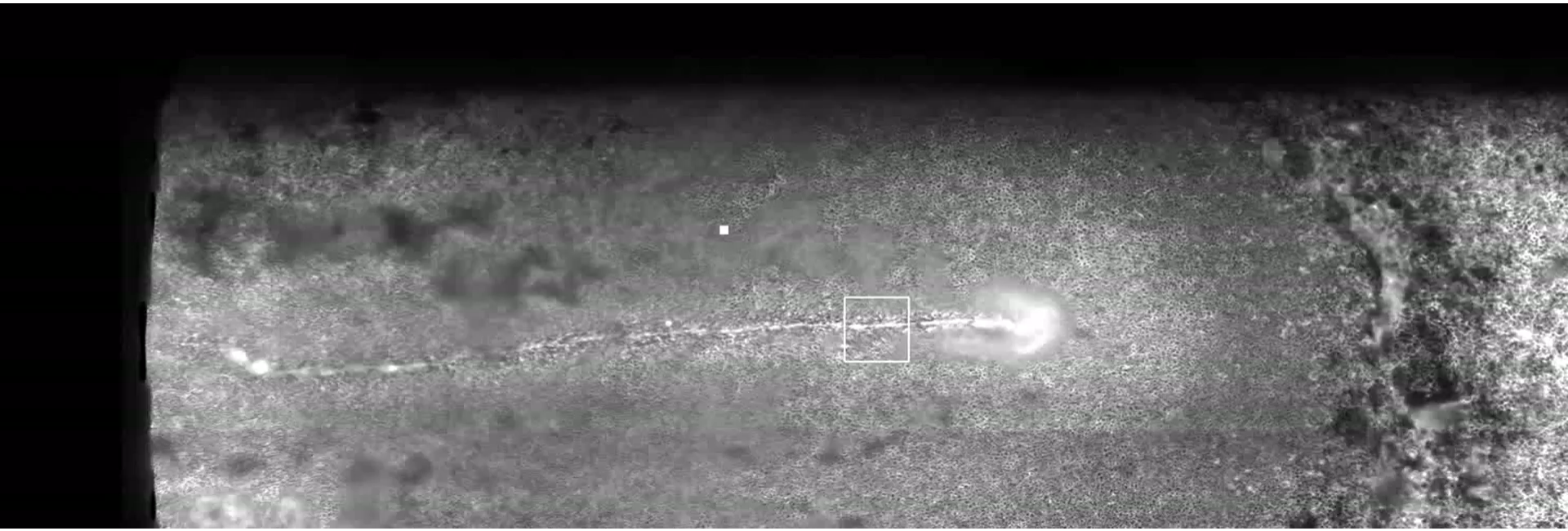

Dictyostelium:
Chemotaxis towards cAMP

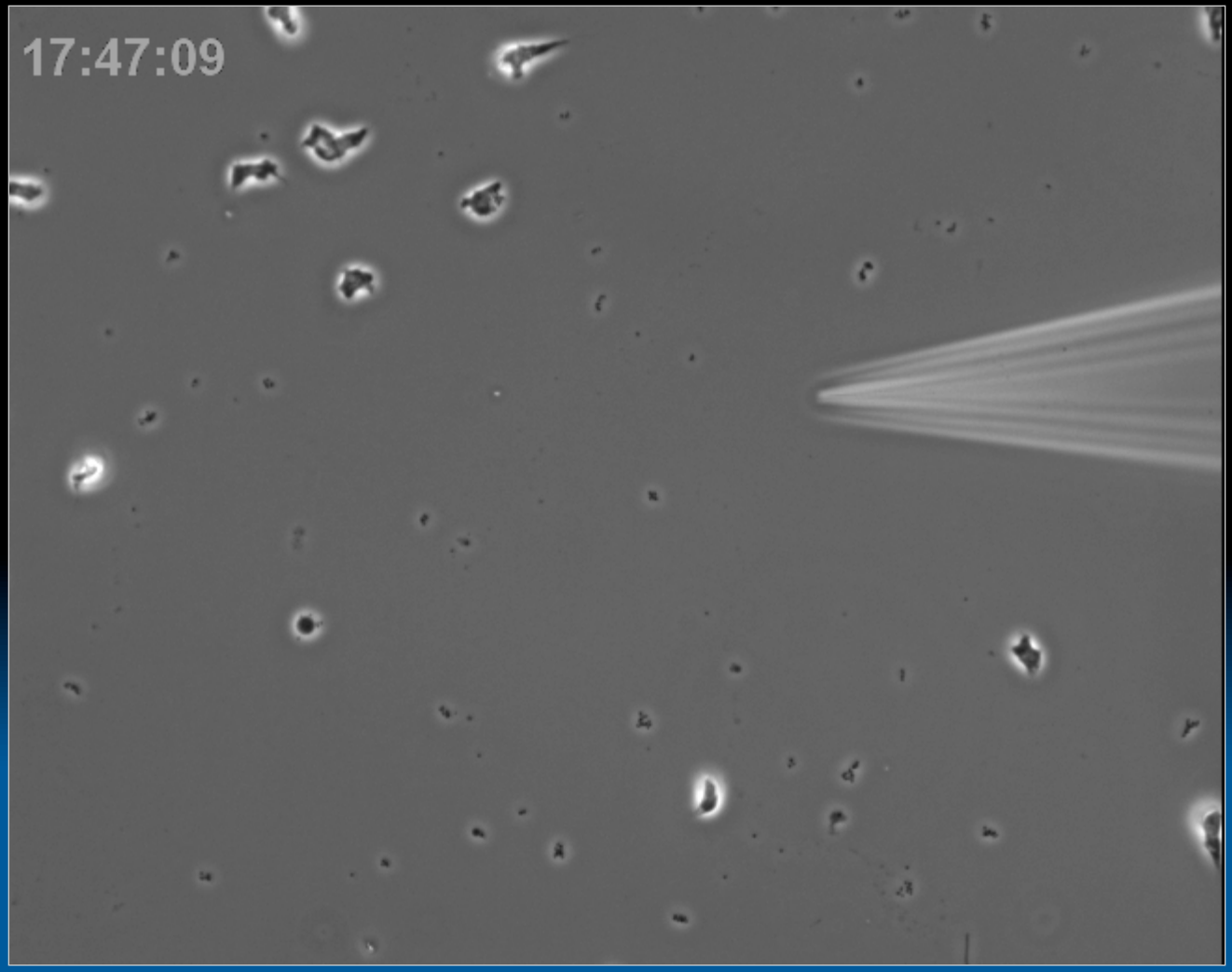

(Hans Faix)

Dictyostelium Chemotaxis: Actin-Assembly at the Front and Myosin-II Recruitment to the Tail

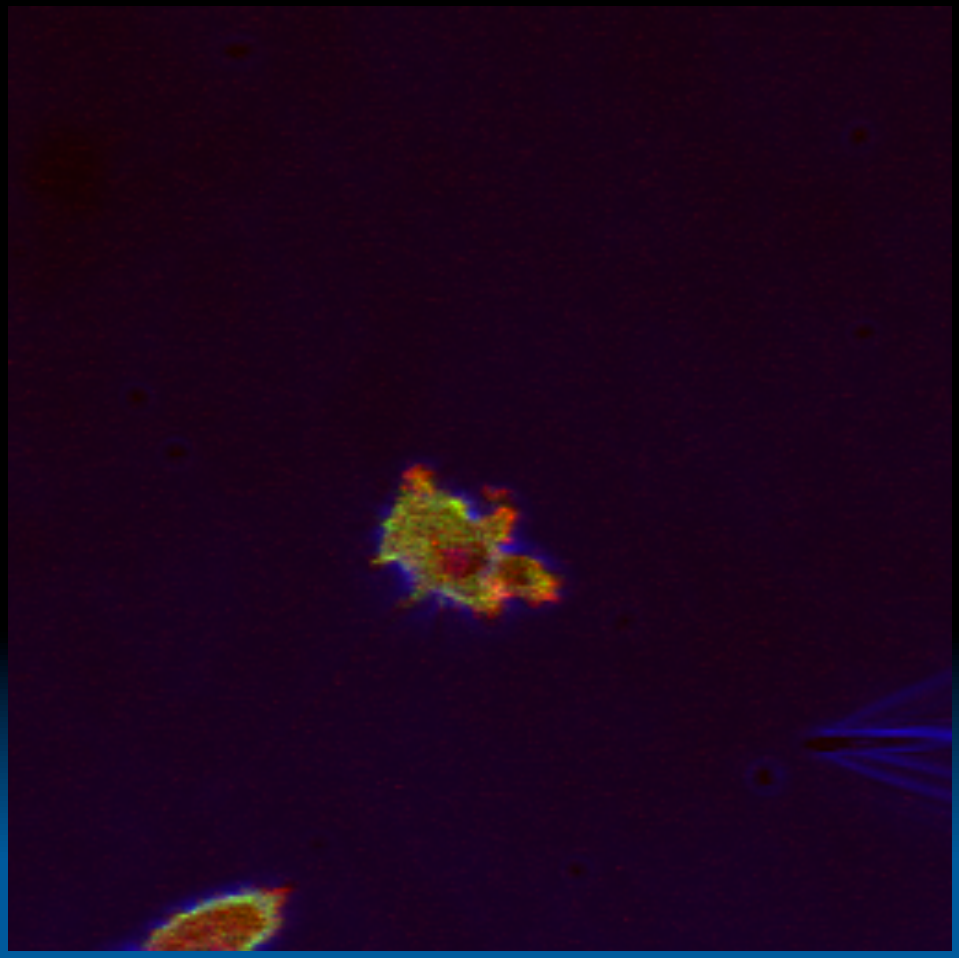

Red: Polymerized actin
(mRFP-LimE Δ coil probe)

Green: Myosin II
(GFP – heavy chain)

Frame interval: 5 seconds

movie by J. Dalous

WARWICK

Regulation of Actin polymerization at the front and Myosin-II contraction at the rear

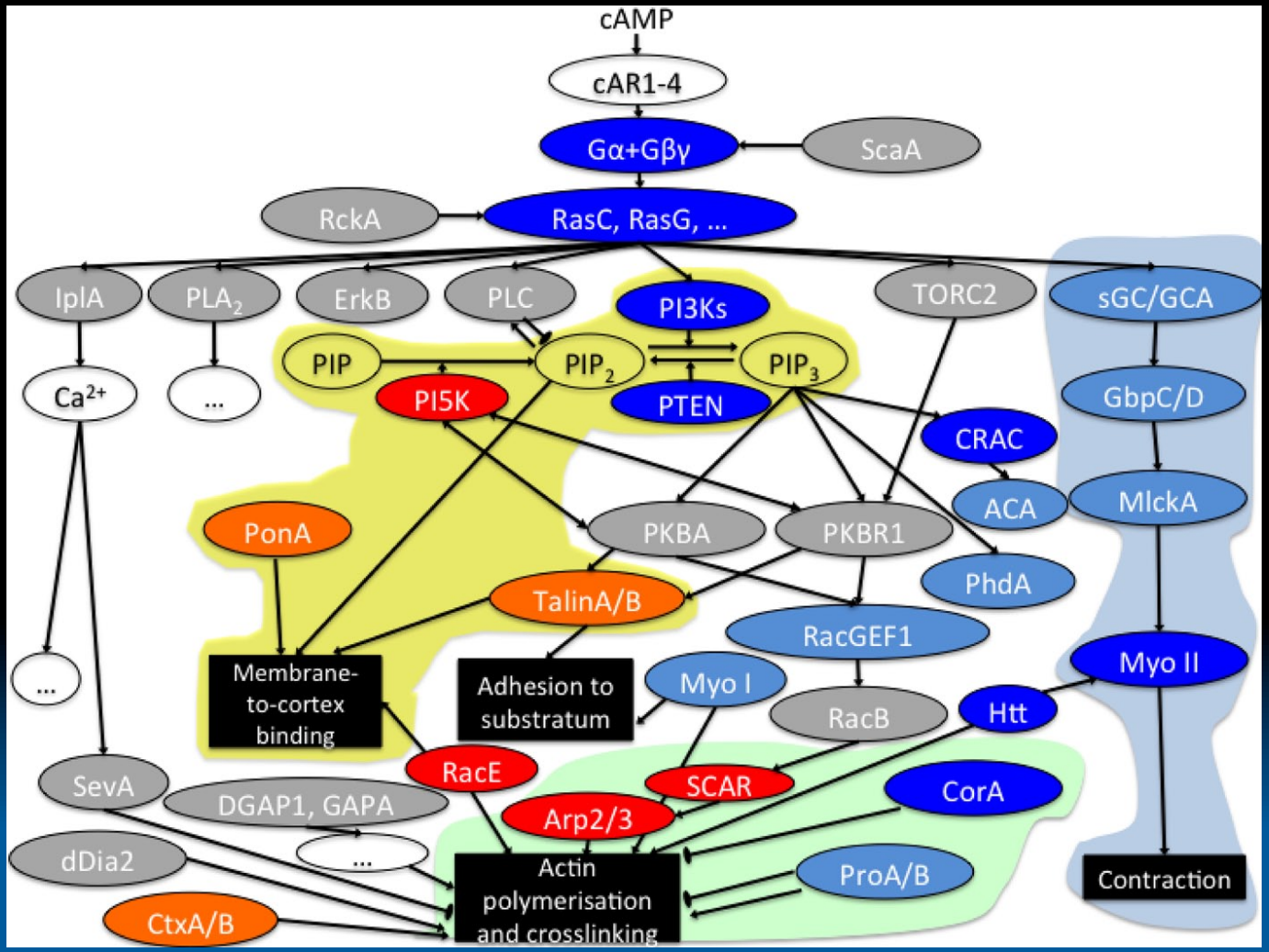

Zatulovskiy, Tyson, Bretschneider & Kay. JCB, 2014

WARWICK

Questions

How can we extract quantitative data of complex spatio-temporal dynamics?

Can we use mathematical modelling to understand the most basic circuitry underpinning cell polarisation?

Do unique solutions exist for a particular model?

WARWICK

Response of *Dictyostelium* to shear flow

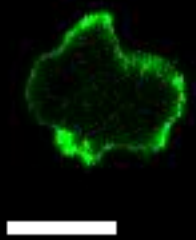

Ingrid Tigges, Warwick

Polarity reversal at high shear-stresses (2.1 Pa)

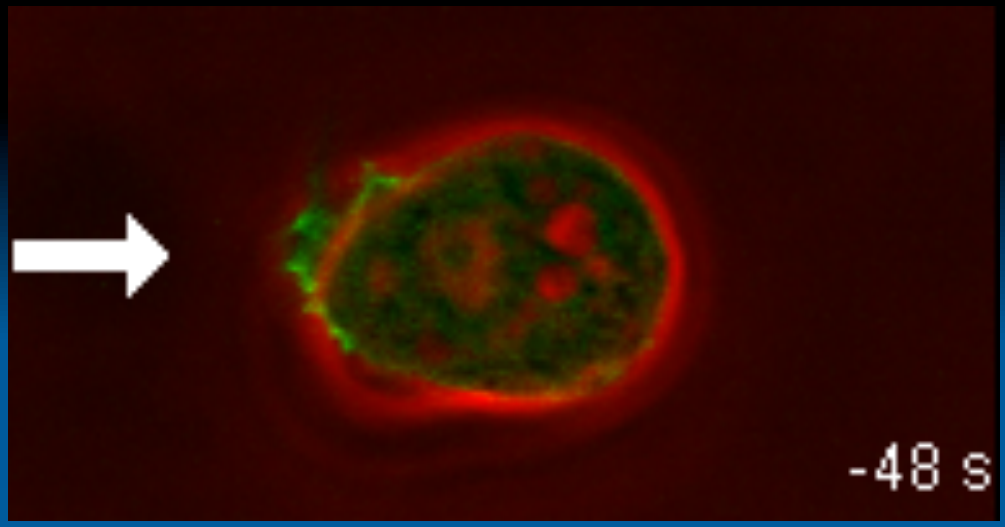

green: Actin label
red: phase contrast

WARWICK

with G. Gerisch & F. Bruckert: Dalous et al., Biophys. J., 2008

Meinhardt

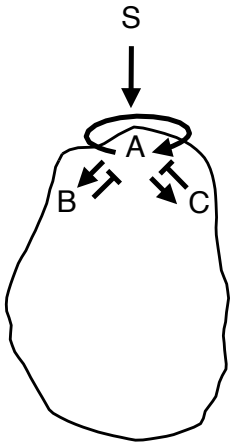

$$\frac{\partial A}{\partial t} = \frac{sr_a\left(\frac{A^2}{B} + b_a\right)}{(s_c + C)(1 + s_a A^2)} - r_a A + D_A \frac{\partial^2 A}{\partial x^2}$$

$$\frac{dB}{dt} = r_b \sum_n \frac{A}{n} - r_b B$$

$$\frac{\partial C}{\partial t} = b_c A - r_c C + D_C \frac{\partial^2 C}{\partial x^2}$$

Levchenko/Iglesias

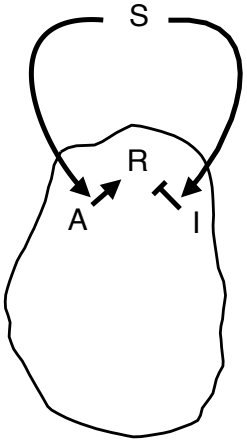

$$\frac{\partial A}{\partial t} = k_A s - k_{-A} A$$

$$\frac{\partial I}{\partial t} = k_I s - k_{-I} I + D \frac{\partial^2 I}{\partial x^2}$$

$$\frac{\partial R}{\partial t} = k_R A(R_T - R) - k_{-R} IR$$

Otsuji

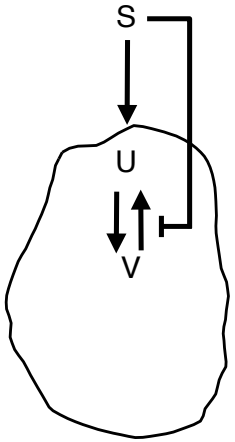

$$\frac{\partial U}{\partial t} = a_1 \left[V - \frac{U + V}{(a_2 s(U + V) + 1)^2} \right] + D_u \frac{\partial^2 U}{\partial x^2}$$

$$\frac{\partial V}{\partial t} = a_1 \left[\frac{U + V}{(a_2 s(U + V) + 1)^2} - v \right] + D_v \frac{\partial^2 U}{\partial x^2}$$

$$s = (1 + dycos(2\pi x))$$

s: external signal, dy is a free parameter to start with

Model Fitting

- Implementation in PottersWheel (MATLAB)
- Experimental data: Activator variable resembles actin fluorescence sampled at P=20 points in the cell cortex
- 1D PDE model on a closed circle (periodic boundary conditions)
- Finite difference discretization

$$\partial^2 C_i / \partial x^2 \approx (C_{i-1} - 2C_i + C_{i+1}) / (\Delta x)^2$$

- N-variable PDE problem is expressed as system of PxN ODEs
- Standard ODE solvers (RK45) and NLLS methods (Gauss Newton Trust-region) for fitting can be used

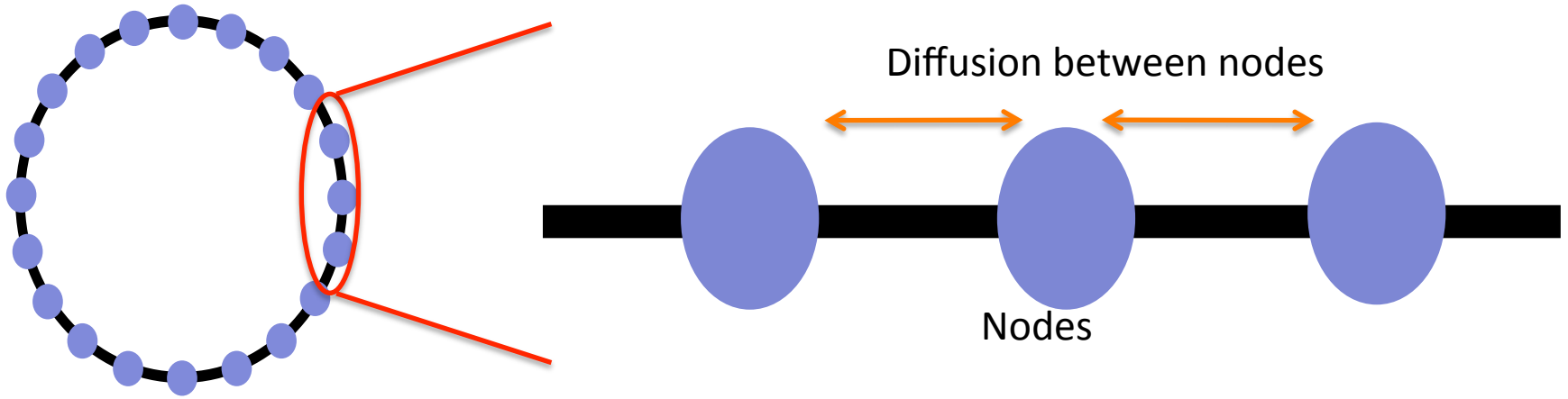

Fitting the Meinhardt model to averaged time course data

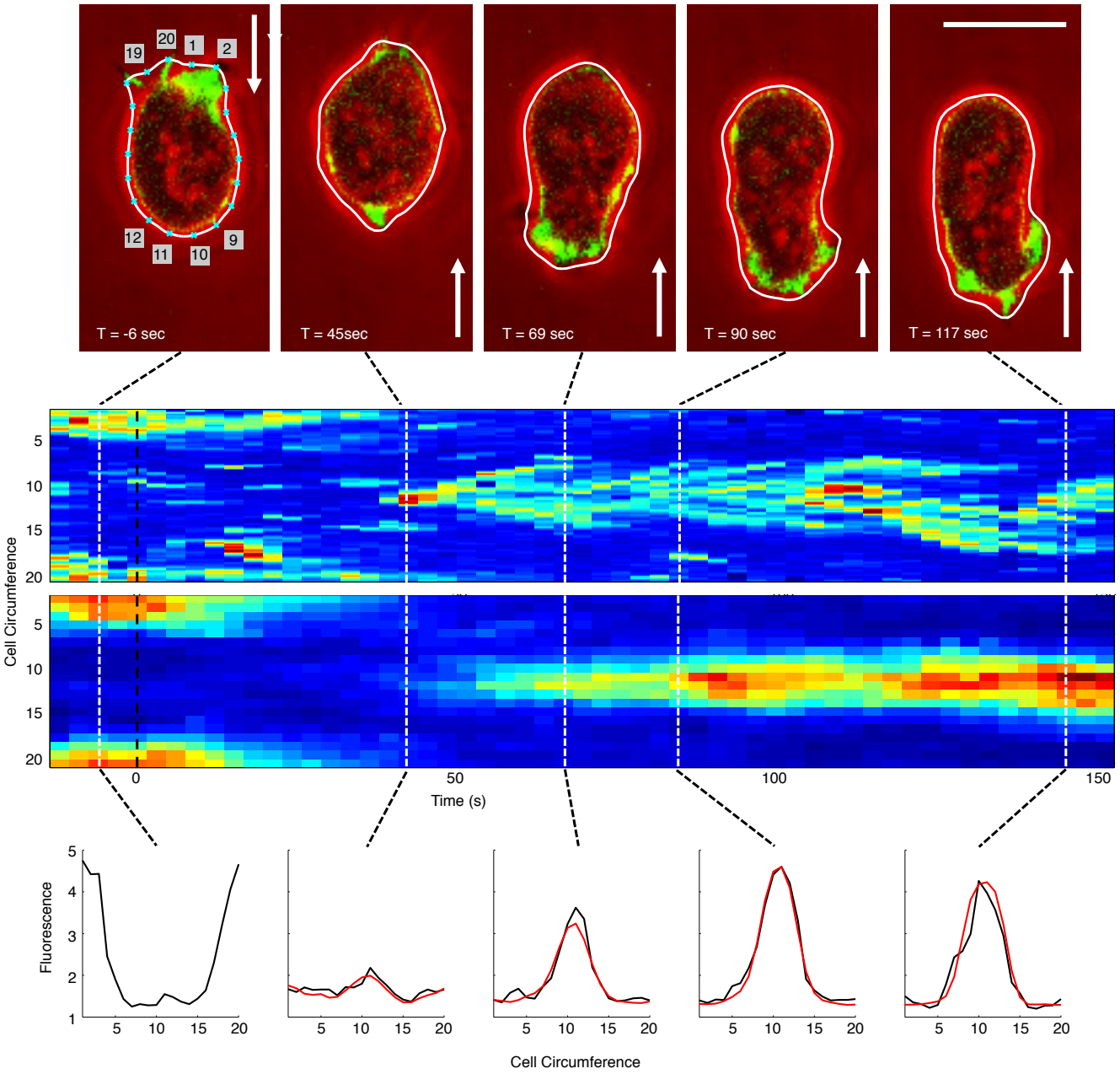

Simultaneous fitting of three experimental conditions

Red: emerging new front, black: linearly decaying old front

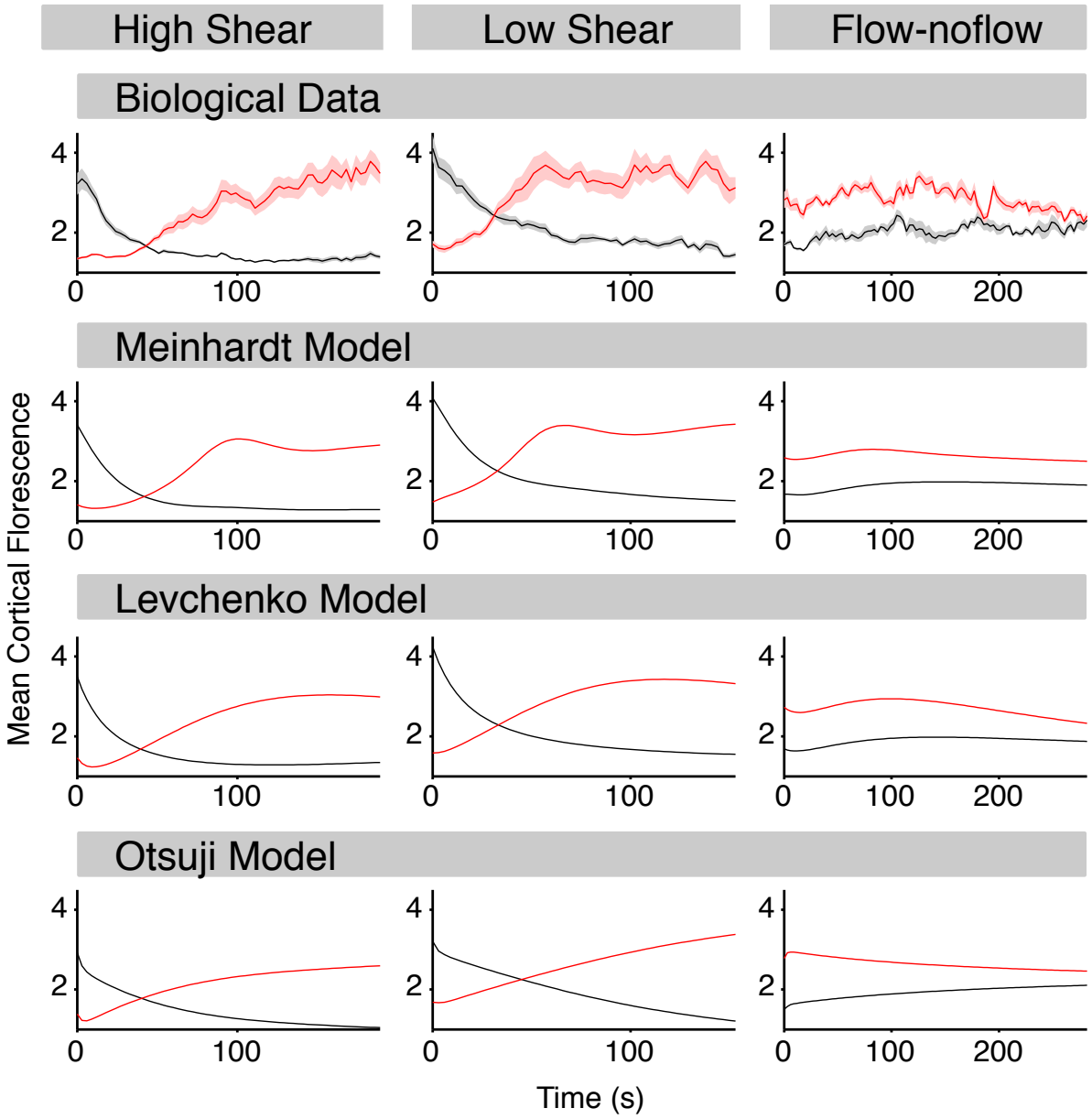

Identifiability analysis: Profile likelihood estimation

Meinhardt Model

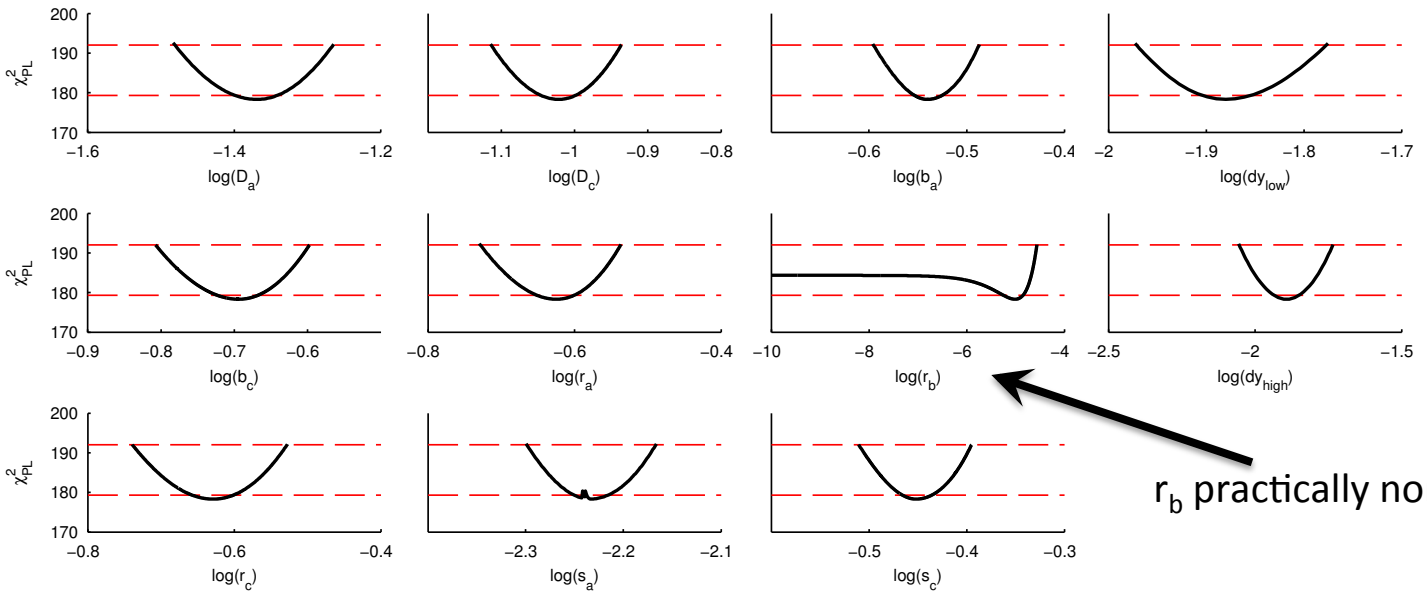

r_b practically non identifiable

Levchenko Model

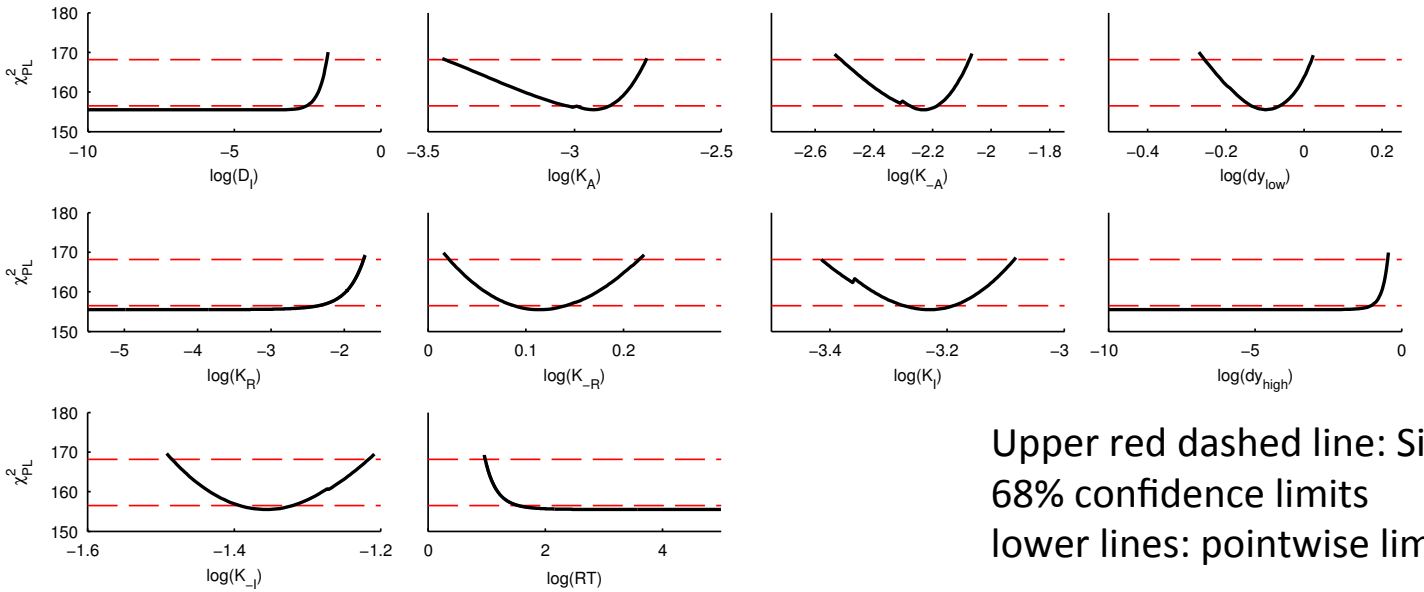

Upper red dashed line: Simultaneous 68% confidence limits
lower lines: pointwise limits

Reducing the Meinhardt model

- Inhibitor B turns out to stay almost constant
- replace it by $B(P)=1+\beta_0(P^2+\beta_1 P)$ where P is the pressure in Pascal
- dy(P=0) = 0, and dy(P) = const

$$\frac{\partial A}{\partial t} = \frac{sr_a\left(\frac{A^2}{B}+b_a\right)}{(s_c+C)(1+s_aA^2)} - r_aA + D_A\frac{\partial^2 A}{\partial x^2}$$

$$\frac{dB}{dt} = r_b\sum_n \frac{A}{n} - r_bB$$

$$\frac{\partial C}{\partial t} = b_cA - r_cC + D_C\frac{\partial^2 C}{\partial x^2}$$

$$s = (1+dycos(2\pi x))$$

original

$$\frac{\partial A}{\partial t} = \frac{sr_a\left(\frac{A^2}{B(P)}+b_a\right)}{(s_c+C)(1+s_aA^2)} - r_aA + D_A\frac{\partial^2 A}{\partial x^2}$$

$$\frac{\partial C}{\partial t} = b_cA - r_cC + D_C\frac{\partial^2 C}{\partial x^2}$$

$$s = (1+dy(P)cos(2\pi x))$$

modified

Removing inhibitor B from the Meinhardt model

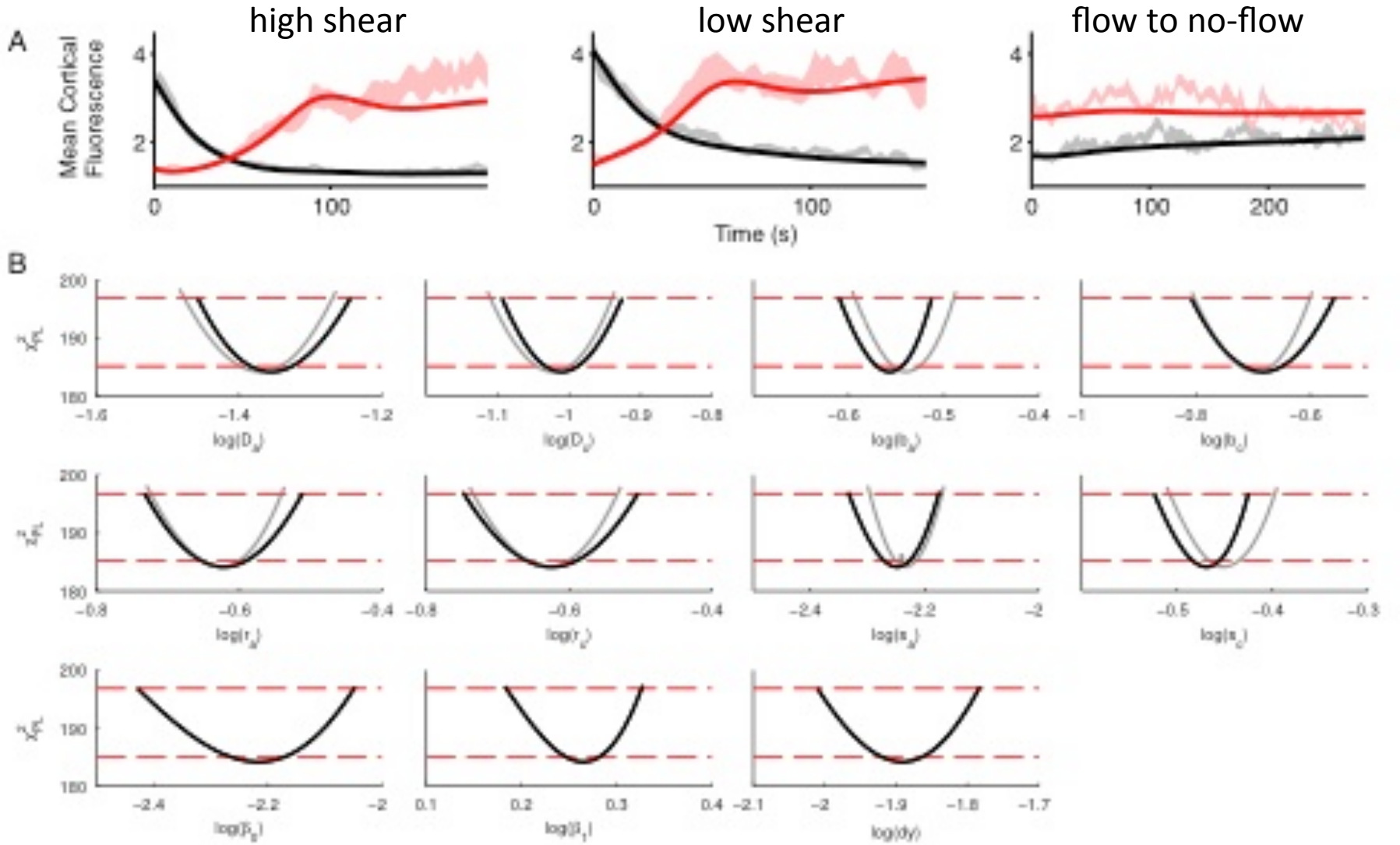

Making predictions: stable movement at P=1Pa

Levchenko
(significant parameter change required)

2-variable Meinhardt
(parameters as before: front splits in three)

2-variable Meinhardt with D_C decreased by 20%

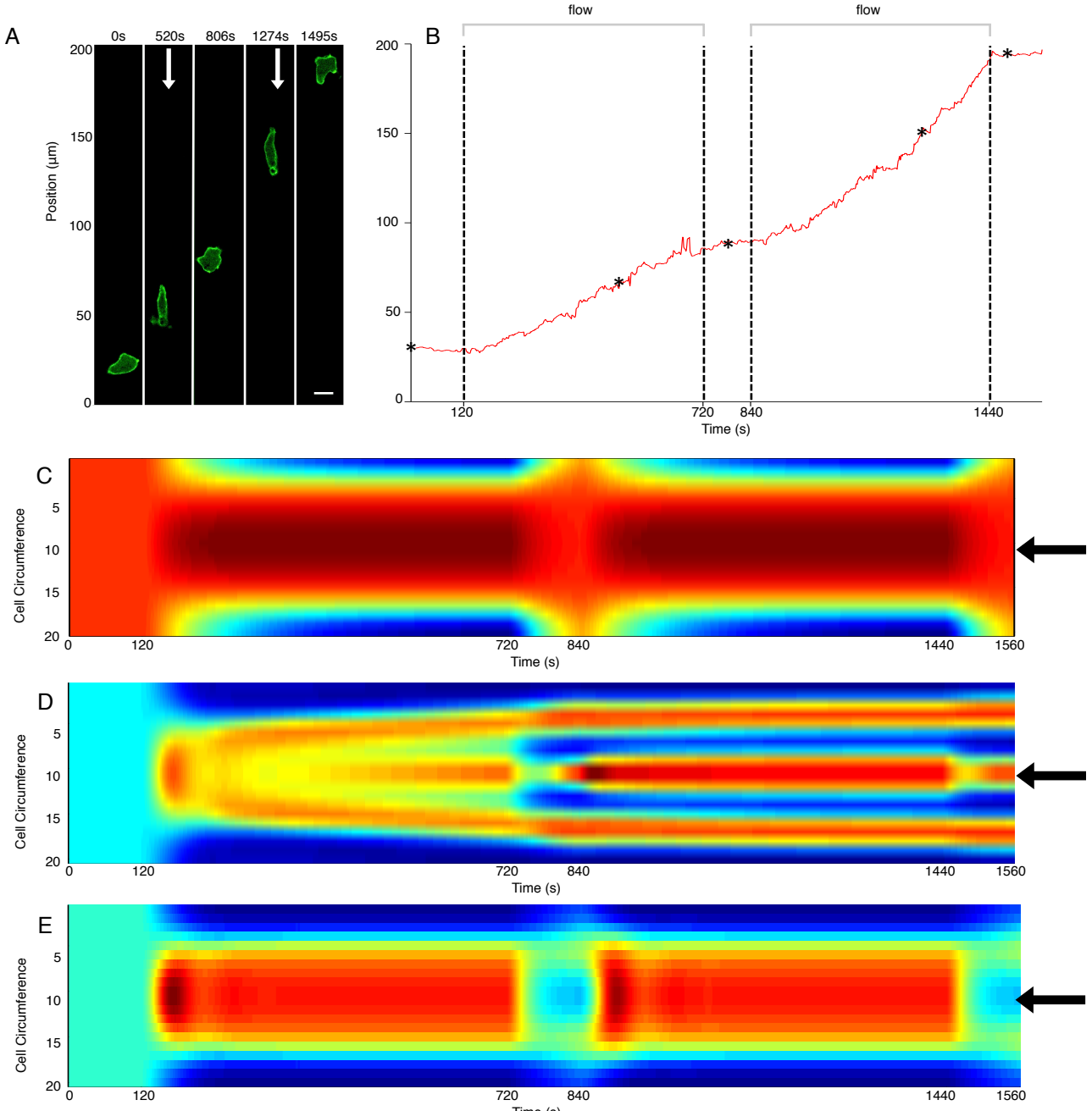

Fitting spontaneous movement of single cells

(convolution performed by deterministic PDE models helps interpreting the underlying stochastic process, estimating timescales of how determined a system actually is)

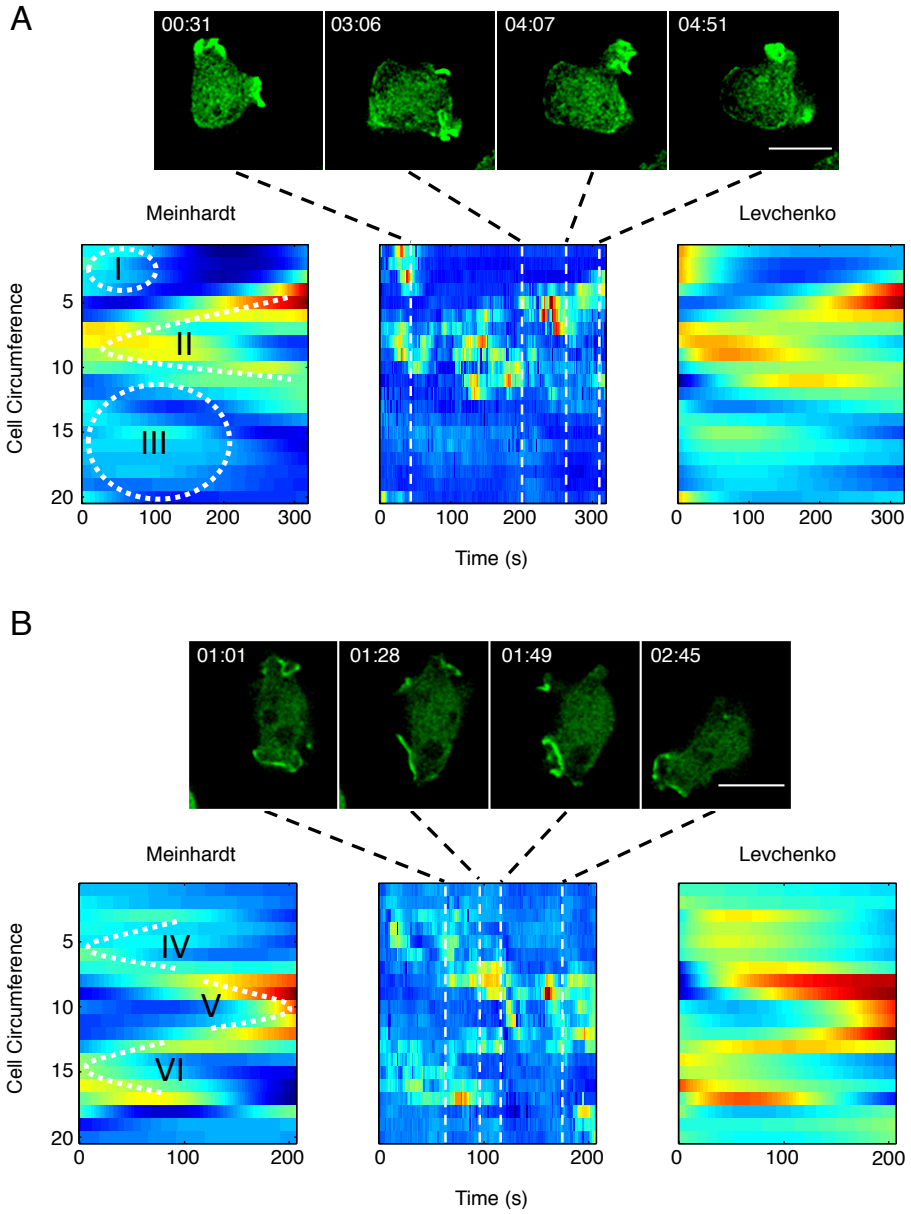

Parameters

Original Meinhardt 3-variable		Meinhardt 2-variable (identifiable)		Meinhardt 2-variable Single stable front		Meinhardt 2-variable Random motility	
D_A	4.274×10^{-2}	D_A	4.415×10^{-2}	D_A	4.415×10^{-2}	D_A	2.311×10^{-3}
D_C	9.513×10^{-2}	D_C	9.768×10^{-2}	D_C	7.064×10^{-2}	D_C	1.471×10^{-8}
b_a	0.2881	b_a	0.2776	b_a	0.2776	b_a	0.1438
b_c	0.2022	b_c	0.2076	b_c	0.2076	b_c	5.643×10^{-2}
r_a	0.2371	r_a	0.2393	r_a	0.2393	r_a	9.467×10^{-2}
r_c	0.2346	r_c	0.2378	r_c	0.2378	r_c	6.552×10^{-2}
s_a	5.833×10^{-3}	s_a	5.647×10^{-3}	s_a	5.647×10^{-3}	s_a	3.054×10^{-3}
s_c	0.3534	s_c	0.3397	s_c	0.3397	s_c	0.2791
r_b	1.000×10^{-5}						
		β_0	6.081×10^{-3}	β_0	6.081×10^{-3}		
dy_{low}	1.318×10^{-2}	β_1	1.840	β_1	1.840		
dy_{high}	1.281×10^{-2}	dy	1.280×10^{-2}	dy	1.280×10^{-2}		

Summary Reorientation

- Well-established tools (Potterswheel) for fitting systems of ODEs can be used to fit reaction-diffusion models. The most simple approach is based on a finite-difference discretization of the diffusion operator.
- Profile likelihood estimations helps immensely to evaluate the identifiability of models.
- Two popular models for cell orientation (Meinhardt and Levchenko) fit similarly well. A reduced version of the Meinhardt model is fully identifiable.
- Predictions help to further constrain parameters. Long term stability of single fronts can be achieved by a 20% reduction of D_C, the diffusion constant of the inhibitor.
- We are able to fit single cell data of randomly migrating cells. Because they need to produce simultaneous fronts, the derived parameter set is significantly changed.

Migration under agarose induces blebbing in Dictyostelium

with Evgeny Zatulovskiy, Rob Kay
(MRC LMB, Cambridge)

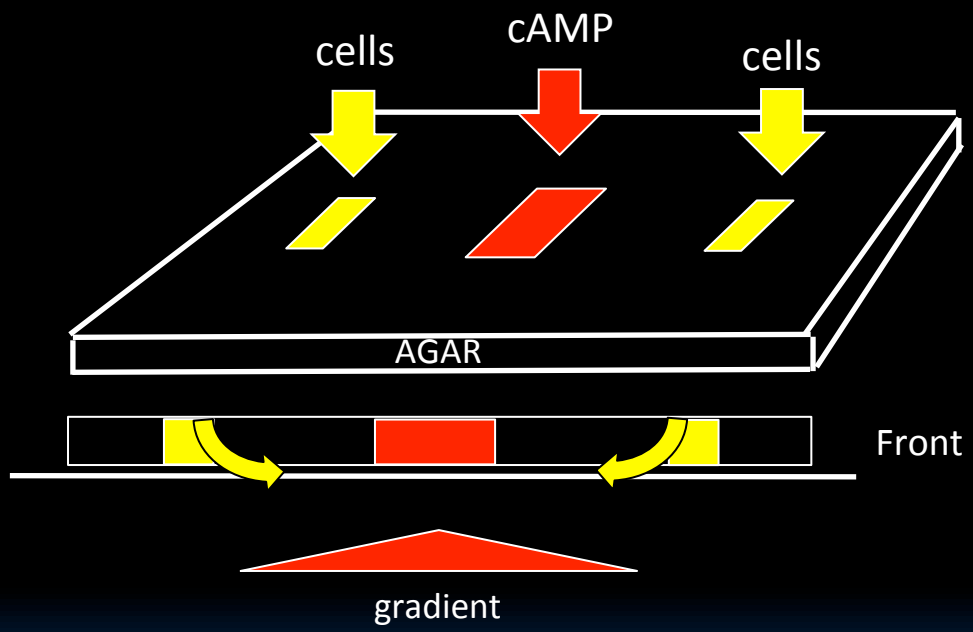

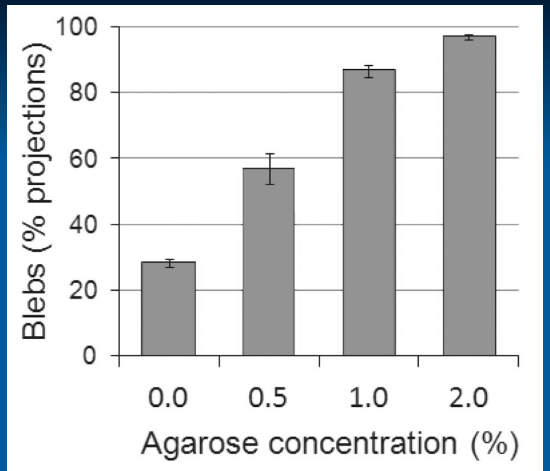

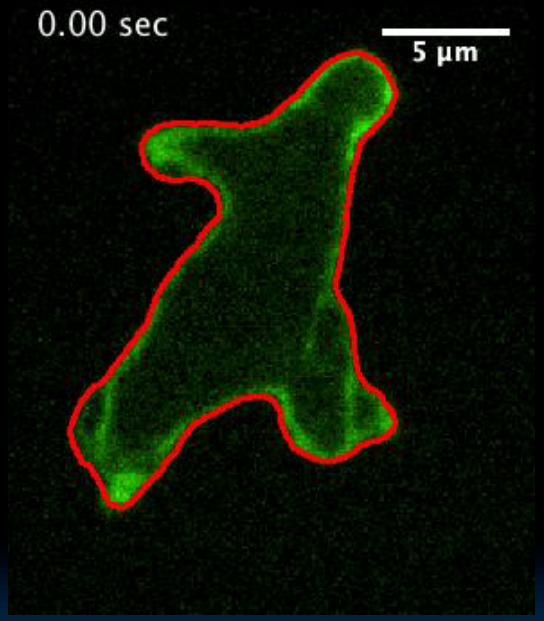

F-actin marker: GFP-ABD (ABP-120)

Spinning disk microscopy (4.5 fps)
Confocal microscopy (2 fps)

Tyson, Zatulovskiy, Kay & Bretschneider, PNAS 2014

Blebbing is driven by Myosin-II dependent pressure

M2 melanoma cell line

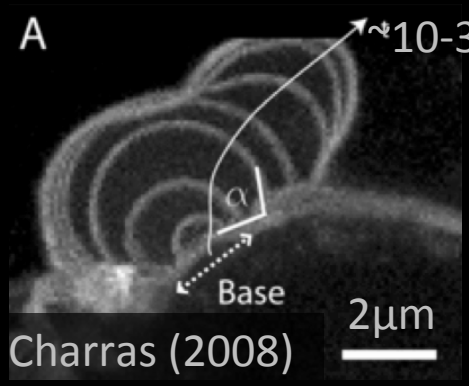

Charras (2008)

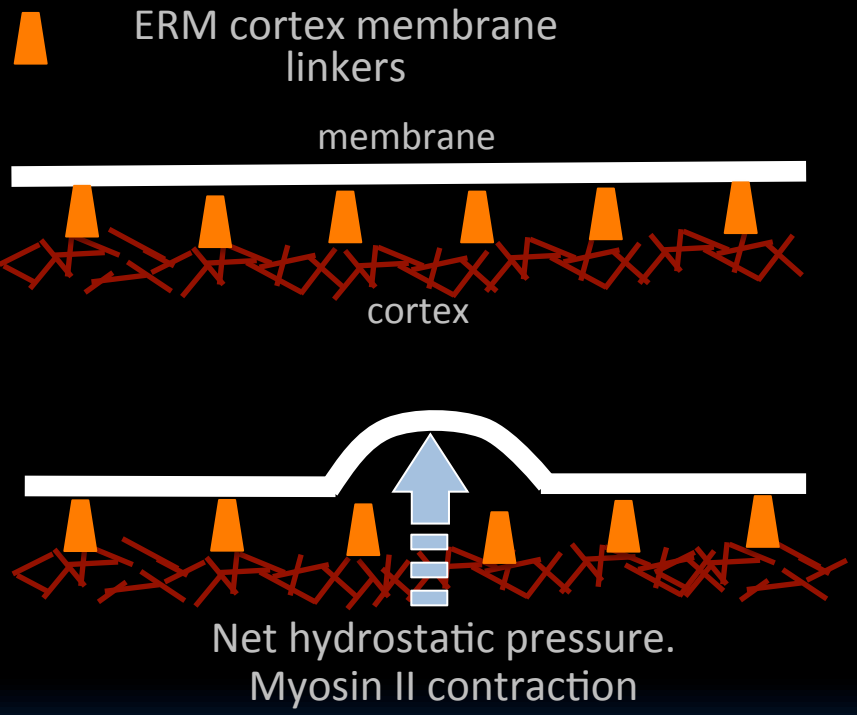

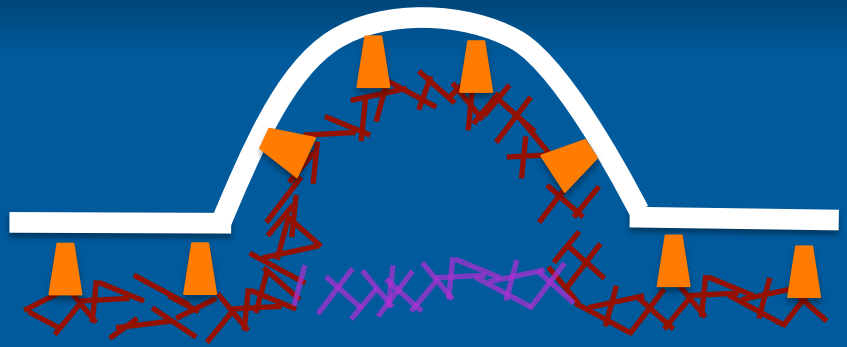

Cellular blebbing

- Myosin-II dependent, driven by hydrostatic pressure
- Often found in cells moving in 3D constrained environments (zebrafish primordial germ cells, tumor cell migration)

How can cells direct blebs to the cell front? How do blebs and actin based protrusions interact?

- Previously known regulators of bleb site selection: Weakening of the acto-myosin cortex, local contraction of myosin-II, asymmetric distribution of membrane-cortex linkers
- New: Cell geometry and membrane tension are important factors in bleb site selection, too

ECMM-APT: Automatic Protrusion Tracking

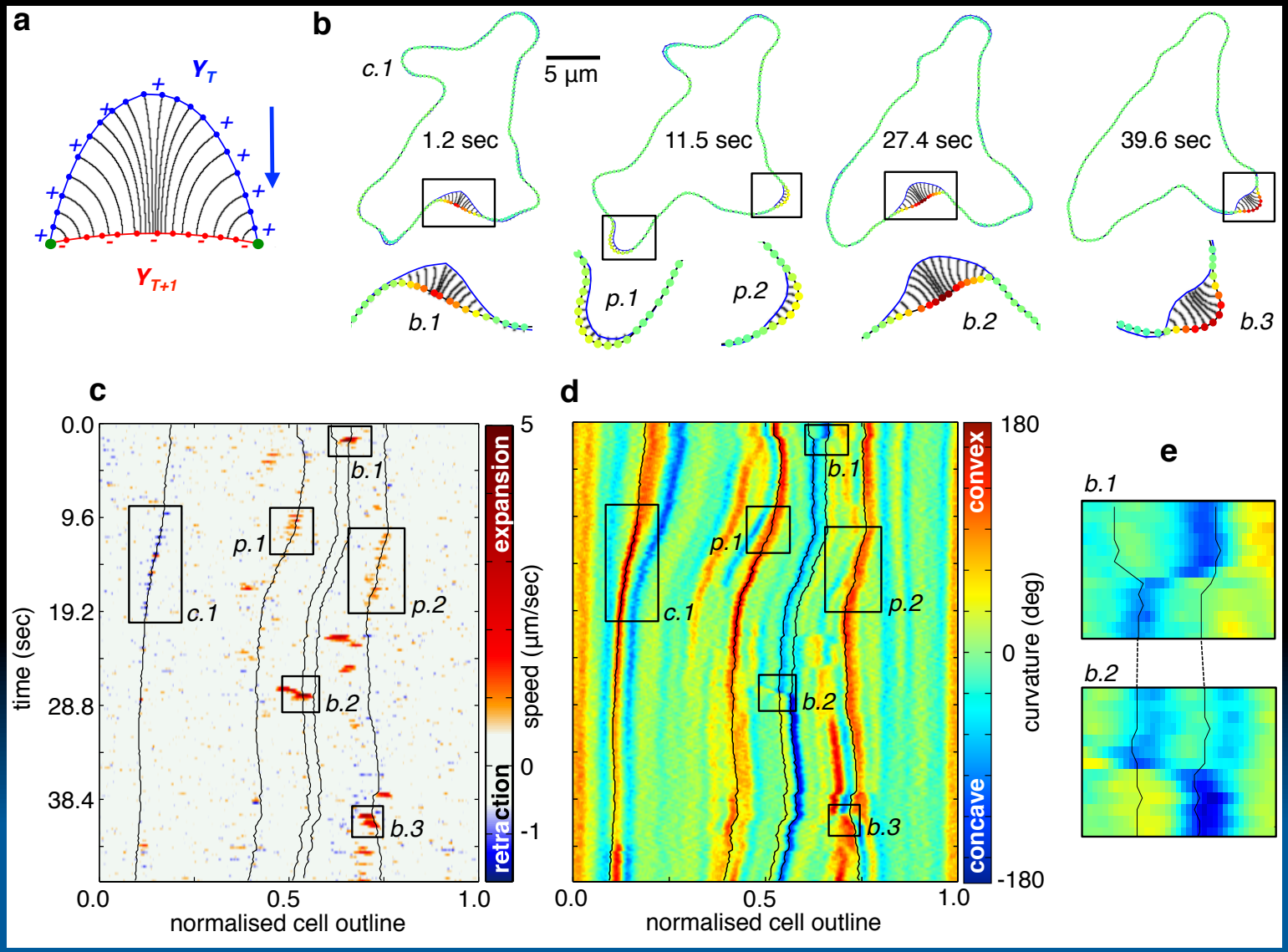

WARWICK

Negative curvature promotes blebbing

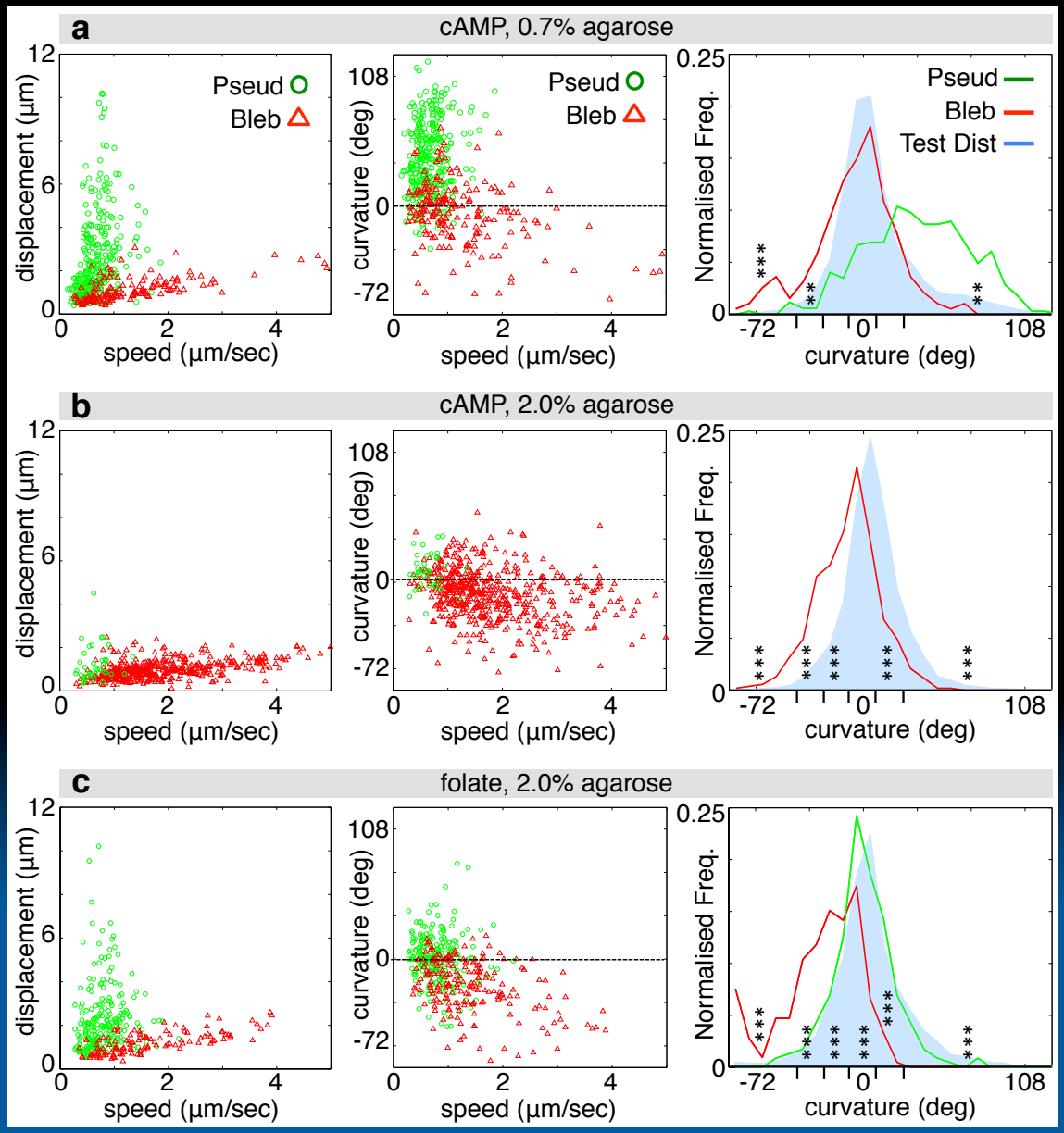

Blebs Nucleate at the Flanks (Armpits) During Chemotaxis

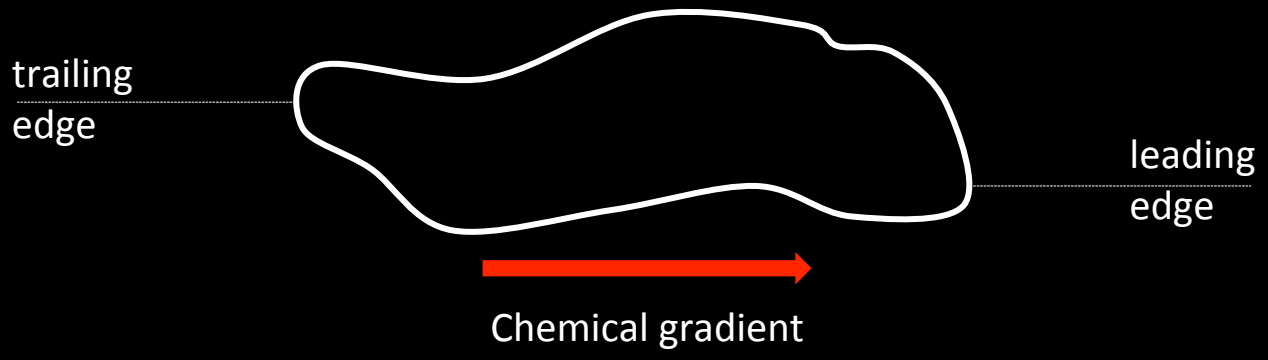

Frequency of Actin-driven Pseudopodia Nucleation

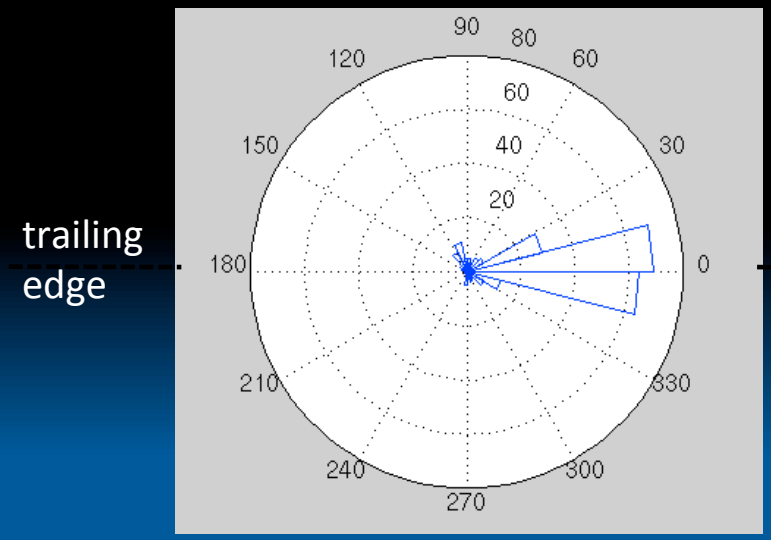

Frequency of Bleb Nucleation

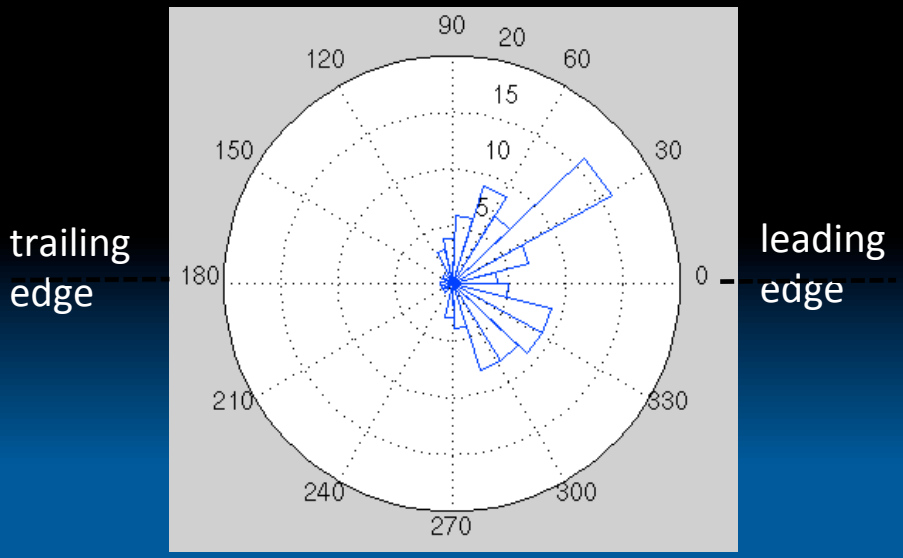

WARWICK

Chains of blebs under 2% agarose (bleb only mode)

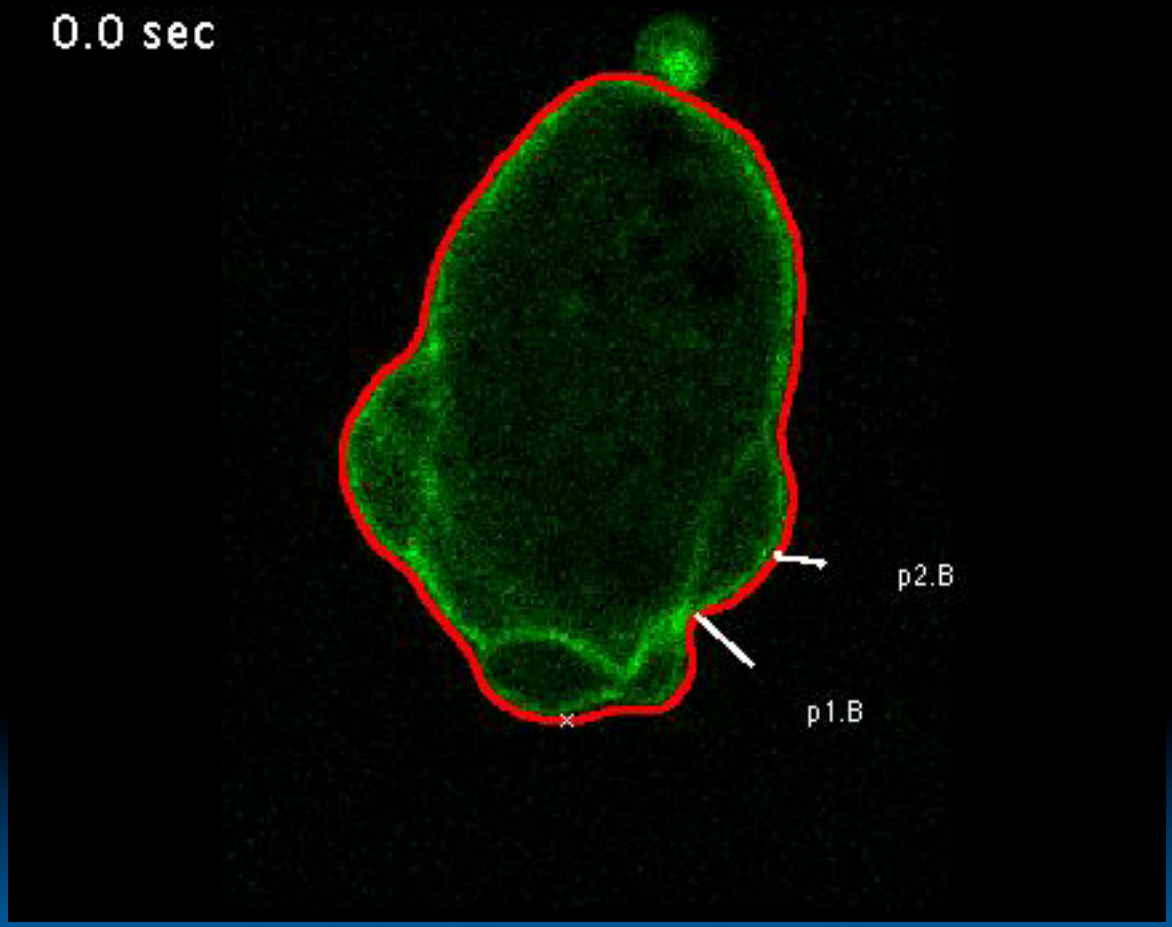

WARWICK

Actin driven protrusions can localize bleb nucleation in *Dictyostelium*

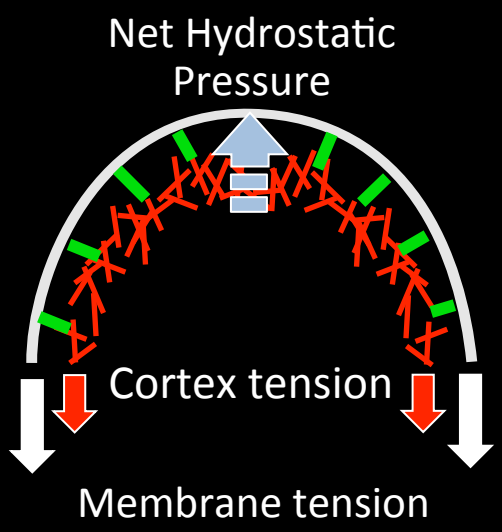

Convex

F-actin drives the formation of blebs by inducing curvature

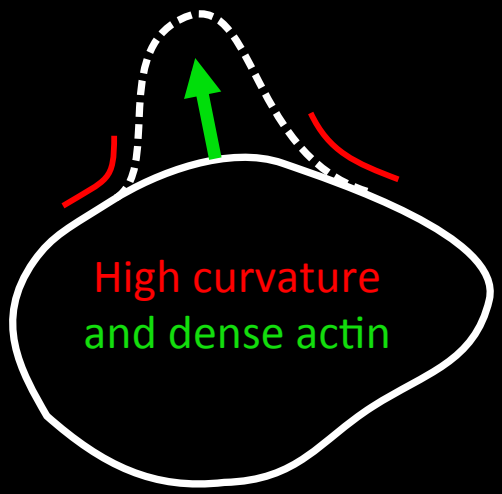

Concave

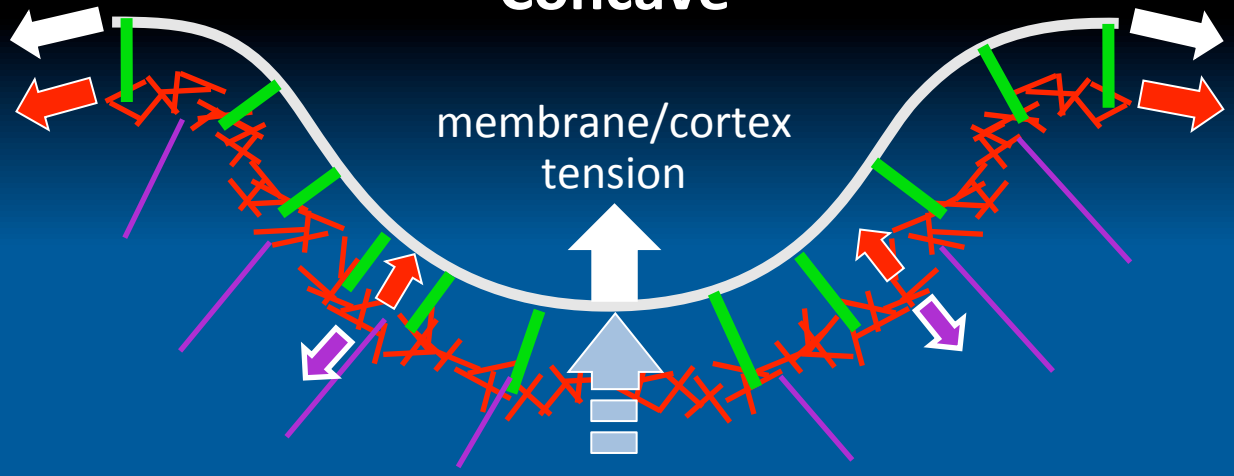

A biomechanical model for bleb initiation

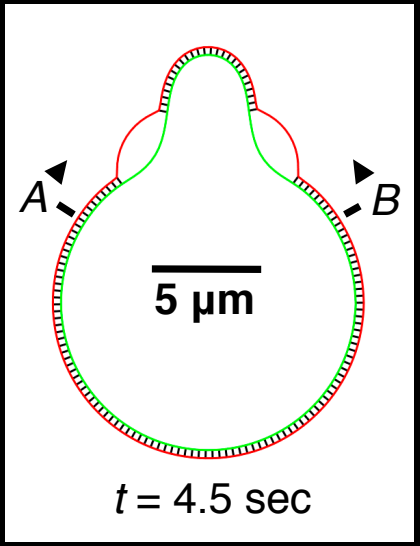

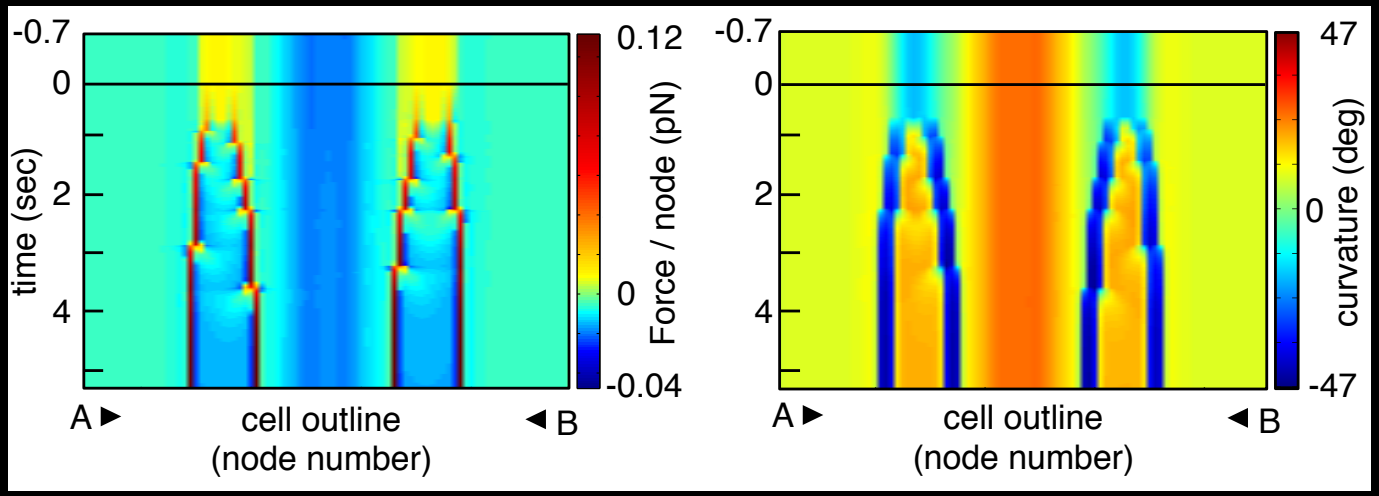

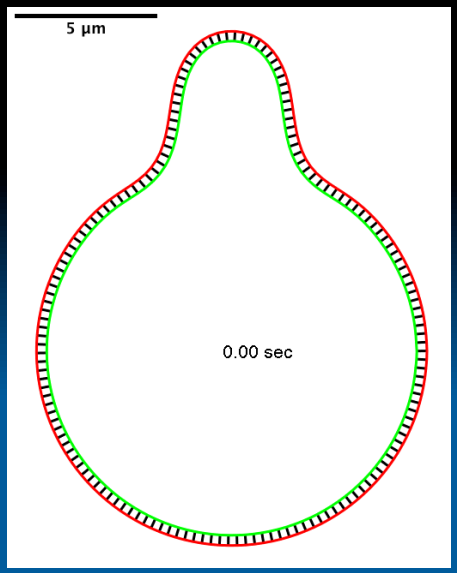

Forces: Membrane tension, bending rigidity, intracellular pressure, Hookean springs link membrane and cortex. Linkers break above certain length.

Actin cortex is considered fixed during blebbing, no regrowth of actin cortex at the naked membrane.

WARWICK

Blebbing of Fundulus deep cells maintaining a highly curved waist

WARWICK

Kindly provided by Rachel Fink, Mount Holyoke College

Summary Blebbing

Long term goal: Linking biochemistry and mechanics

- Actin provides a force pushing the cell membrane outward, and increases membrane tension. Work by Orion Weiner and others has shown that membrane tension quenches protrusive activity at the cell rear (long range inhibition). Our work shows that tension has a dual role: In concave regions it can also act as a local activator of cellular protrusions in form of blebs.

Current members

Richard Tyson, QuimP, Blebbing in *Dictyostelium*

Chengjin Du, CellTracker: Quantifying transcription factor dynamics, 3D cell reconstructions

Robert Lockley, Modelling cell polarity

Neil Venables: Microtubule dynamics

Alumni

Mike Downey, LineageTracker

Ingrid Tigges, Microfluidics experiments, now working for Mathworks

Main Collaborators

Graham Ladds, Warwick Medical School
Rob Kay, MRC-LMB, Cambridge
Kees Weijer, University of Dundee
Len Stephens, Babraham, Cambridge

BBSRC bioscience for the future
Supported by wellcome trust
EPSRC Engineering and Physical Sciences Research Council
THE ROYAL SOCIETY
THE UNIVERSITY OF WARWICK